2005-12

Optical beam control using adaptive optics

McLaughlin, Lisa

Monterey, California. Naval Postgraduate School

NAVAL POSTGRADUATE SCHOOL

MONTEREY, CALIFORNIA

THESIS

OPTICAL BEAM CONTROL USING ADAPTIVE OPTICS

by

Lisa McLaughlin

December 2005

Thesis Advisor: Brij Agrawal
Co-Advisor: Ty Martinez

Approved for public release; distribution is unlimited

THIS PAGE INTENTIONALLY LEFT BLANK

REPORT DOCUMENTATION PAGE			Form Approved OMB No. 0704-0188
Public reporting burden for this collection of information is estimated to average 1 hour per response, including the time for reviewing instruction, searching existing data sources, gathering and maintaining the data needed, and completing and reviewing the collection of information. Send comments regarding this burden estimate or any other aspect of this collection of information, including suggestions for reducing this burden, to Washington headquarters Services, Directorate for Information Operations and Reports, 1215 Jefferson Davis Highway, Suite 1204, Arlington, VA 22202-4302, and to the Office of Management and Budget, Paperwork Reduction Project (0704-0188) Washington DC 20503.			
1. AGENCY USE ONLY *(Leave blank)*	**2. REPORT DATE** December 2005	**3. REPORT TYPE AND DATES COVERED** Master's Thesis	
4. TITLE AND SUBTITLE: Optical Beam Control Using Adaptive Optics			**5. FUNDING NUMBERS**
6. AUTHOR(S) Lisa McLaughlin			
7. PERFORMING ORGANIZATION NAME(S) AND ADDRESS(ES) Naval Postgraduate School Monterey, CA 93943-5000			**8. PERFORMING ORGANIZATION REPORT NUMBER**
9. SPONSORING /MONITORING AGENCY NAME(S) AND ADDRESS(ES) N/A			**10. SPONSORING/MONITORING AGENCY REPORT NUMBER**
11. SUPPLEMENTARY NOTES The views expressed in this thesis are those of the author and do not reflect the official policy or position of the Department of Defense or the U.S. Government.			
12a. DISTRIBUTION / AVAILABILITY STATEMENT Approved for public release; distribution is unlimited			**12b. DISTRIBUTION CODE**

13. ABSTRACT (maximum 200 words)

Adaptive optics is a new and growing research area aimed at creating high-quality imagery by correcting aberrations in optical systems caused by turbulence in the earth's atmosphere. This paper concentrates on the basics of physical optics leading into the design of an adaptive optics test bed to study the correction of aberrations using optical beam control. Adaptive optics requires the use of sophisticated optical equipment such as deformable mirrors and wavefront sensors.

The experimental portion of the work focuses on using a deformable mirror to control the aberrations in a system using laser light. By using a combination of lenses, deformable mirror, and wavefront sensor, the test bed will correct aberrations induced into a plane wave. In addition, the mechanics and function these components was be explored, setting the building blocks for future studies concerning optical beam control.

14. SUBJECT TERMS Adaptive Optics, Beam Control			**15. NUMBER OF PAGES** 93
			16. PRICE CODE
17. SECURITY CLASSIFICATION OF REPORT Unclassified	**18. SECURITY CLASSIFICATION OF THIS PAGE** Unclassified	**19. SECURITY CLASSIFICATION OF ABSTRACT** Unclassified	**20. LIMITATION OF ABSTRACT** UL

NSN 7540-01-280-5500 Standard Form 298 (Rev. 2-89)
Prescribed by ANSI Std. 239-18

THIS PAGE INTENTIONALLY LEFT BLANK

Approved for public release; distribution is unlimited

OPTICAL BEAM CONTROL USING ADAPTIVE OPTICS

Lisa M. McLaughlin
Lieutenant, United States Navy
B.S., United States Naval Academy, 1997

Submitted in partial fulfillment of the
requirements for the degree of

MASTER OF SCIENCE IN ASTRONAUTICAL ENGINEERING

from the

NAVAL POSTGRADUATE SCHOOL
December 2005

Author: Lisa M. McLaughlin

Approved by: Dr, Brij Agrawal
Thesis Advisor

Dr. Ty Martinez
Co-Advisor

Anthony J. Healey
Chairman, Department of Mechanical and Astronautical Engineering

THIS PAGE INTENTIONALLY LEFT BLANK

ABSTRACT

Adaptive optics is a new and growing research area aimed at creating high-quality imagery by correcting aberrations in optical systems caused by turbulence in the earth's atmosphere. This paper concentrates on the basics of physical optics leading into the design of an adaptive optics test bed to study the correction of aberrations using optical beam control. Adaptive optics requires the use of sophisticated optical equipment such as deformable mirrors and wavefront sensors.

The experimental portion of the work focuses on using a deformable mirror to control the aberrations in a system using laser light. By using a combination of lenses, deformable mirror, and wavefront sensor, the test bed will correct aberrations induced into a plane wave. In addition, the mechanics and function these components was be explored, setting the building blocks for future studies concerning optical beam control.

THIS PAGE INTENTIONALLY LEFT BLANK

TABLE OF CONTENTS

LIST OF FIGURES

LIST OF TABLES

THIS PAGE INTENTIONALLY LEFT BLANK

ACKNOWLEDGMENTS

I would like to express my appreciation to Professor Brij Agrawal for his guidance throughout this project. His support and encouragement made it possible to achieve what seemed impossible. Thank you.

I would also like to thank Sergio Restaino and Ty Martinez for their constant help and encouragement. I greatly appreciate their expert guidance and invaluable assistance with this thesis the time they took to give me experience in their own laboratory. They made this project interesting and fun. I would also like to thank the people at Starfire Optical Range for helping me to adapt concepts to real ideas and for inspiring me to pursue this research.

Finally, I would like to thank Professor Lazarra and Professor Walters for their help patience in helping me to understand the underlying principles of optics.

THIS PAGE INTENTIONALLY LEFT BLANK

I. INTRODUCTION

In the last few decades, the US military has begun to redefine the way it looks at space and its assets. More emphasis has been put on satellite imagery in both military and civilian applications. It is increasingly important to be able to take un-aberrated images from both ground stations and satellites. Much of the image aberration take place in the earth's atmosphere. Steps have been taken recently to correct this using adaptive optics.

Adaptive Optics first got its start in 215 AD with the destruction of the Roman Fleet by Archimedes (Lamberson). He used the reflection of the sun and his solder's shields to direct very intense beam of light toward the oncoming ships in order to ignite the wood and cause the ship to burn, defeating the armada. Later, in the 1730's Newton described what he saw as atmospheric limitation of astronomy causing aberrations of images observed through telescopes. In his works *Optiks* (Newton, 111), he said "Long Telescopes may cause Objects to appear brighter and larger than short ones can do, but they cannot be so formed as to take away that confusion of the Rays which arises from the Tremors of the Atmosphere."

In the early 1950's an astronomer working at the California Institute of Technology proposed a way to compensate for the atmospheric aberrations that caused pictures taken by telescopes to appear blurry or out of focus. He proposed combining a rotating knife edge with a phase corrector along with a mirror coated with a thin controllable oil film so he could control atmospheric turbulence in real time. Due to lack of funds and interest at the time, his research did not progress.

It wasn't until the 1970's that the need for optical correction systems gave way to research and development in adaptive optics. Up until this time, researchers relied mostly on post processing techniques. In the late 1960's the US Air Force began working with the University of Arizona to find a way to improve image quality of pictures of satellites taken from the earth. They began doing experiments using the standard Hartmann test. In this test, large pieces of cardboard with an array of holes were placed over the telescope aperture. Using photographic plates, an image would be produced. By

taking two images a specific distance apart, the rays of the image could be traced in order to calculate the figure of merit for large telescopes. The research team found that by placing a beam splitter in collimated space behind the eyepiece and placing a plate with holes in it at the image of the pupil they could simulate covering up the aperture while taking an image. Unfortunately, this caused the rays from the image to appear blurry and made it more difficult to pinpoint the centroid of the ray. One of the researchers on this team, Dr. Roland Shack, determined that if he exchanged the holes in the cardboard pieces with lenses, then the incoming rays would be more focused. Using this method, they were able to measure wavefront error at the time the image was taken. This sensor system became known as the Shack-Hartmann wavefront sensor and is used in a wide variety of applications today.

A. THESIS OBJECTIVES

Implementing a high-quality laser communications system results in many complications, not the least of which is the quality of the signal. While there are many different solutions to this problem, each with their own issues, many organizations are turning to enhancing the optical quality of the laser beam itself. Proper alignment of the lasing medium and the optical elements is critical for the performance of laser systems. This is being done, in many places through the use of adaptive optics.

The focus of this thesis is to investigate the different laboratories that are currently working on this type of system, lay the foundation for understanding physical optics and adaptive optics, and develop a test bed to understand the underlying physics of optical systems. The ultimate goal of this test bed is to take an incoming light source (laser) and create a cohesive signal by taking out aberrations in the wavefront using deformable mirrors and a wavefront sensor. The test bed will be modeled after test beds currently being used by the Naval Research Laboratory. Research will include the use of a diode-pumped laser, Micro-Machined Deformable Mirror, Piezo-electric Deformable Mirror and Shack-Hartmann wavefront sensor. Knowledge gained from the experimental system will be used in follow-on research leading toward the development of a combined adaptive optics and adaptive controls system.

II. ADAPTIVE OPTICS AS A GROWING RESEARCH FIELD

A. ADAPTIVE OPTICS IN SPACE APPLICATIONS

1. Astronomy

Adaptive Optics were initially developed for use in imaging. As early as the 1700's astronomers understood the limitations of earth-bound telescopes. The study of heavenly bodies became increasingly difficult as astronomers tried to look further and further into space. Much of the difficulty in using earth-bound telescopes stemmed from turbulence in the earth's atmosphere which caused inconsistencies in the refractive index of the air.

In the early 1950's Horace Babcock, an astronomer at the Mount Wilson observatory, proposed a solution to the problem. He proposed using an active optical element such as a mirror to correct the aberrations in the incoming wavefront which would be detected by a sensor that would return a corrective signal to the mirror, completing the system. Due to the limitations in technology in the 1950's he was not able to bring his ideas to fruition until nearly two decades later.

The first adaptive optics system, built at Itek in 1977, was able to enhance two-dimensional images of stars taken with a telescope. This technology paved the way for much larger and more sophisticated systems such as the Air Force's Starfire Optical Range in Albuquerque, NM. Although systems have gotten bigger and more complex, very little has changed from Babcock's original ideas. In his paper "The Possiblilty of Compensated Astronomical Seeing" he described how to use a deformable mirror to compensate for imperfections in a wavefront due to atmospheric aberration. He wrote " If we had a means of continually measuring the deviation of rays from all parts of the mirror, and of amplifying and feeding back this information so as to correct locally the figure of the mirror in response to the schlieren[1] pattern, we could expect to compensate both for seeing and for any inherent imperfections of optical figure." (Babcock,2) Babcock's design, shown below, shows how an image, formed on the orthicon, is

[1] **schlieren**—Parcels or strata of air having densities sufficiently different from that of their surroundings that they may be discerned by means of refraction anomalies in transmitted light. 18 October 2005 <http://amsglossary.allenpress.com/glossary/browse?s=s&p=12>

transferred electronically to the mirror. Deviations in the rays caused by the atmosphere or optical imperfections are corrected using feedback from the mirror. In below diagram, F denotes the field lens and C denotes a guider for centering control of the knife edge, K. The two mirrors shown are off-axis paraboloids.

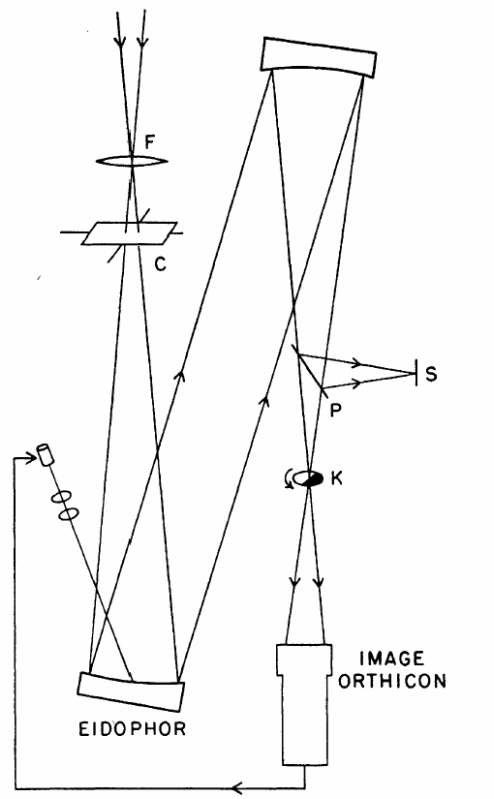

Figure 1. Schematic diagram of seeing compensator[2].

2. Communications

Since the inception of adaptive optics, astronomers all over the world have been using it to enhance the quality of images garnered from space, but new technology has lent the power of adaptive optics systems to space in other ways. One new area of study in adaptive optics has been the coupling of these systems with free space communications using laser beams. Laser communication is a growing area and adaptive optics is already being used in ground-to-ground and ground-to-air communications with future work in ground-to-space.

[2] Babcock, 232.

The future of laser communications systems has four important components: a high power laser, an adaptive optics system for aberration correction, an optical element for pointing and control, and a photovoltaic satellite receiver (Landis). Several issues need to be taken into consideration with a system like this including satellite track, power requirements, mission specific requirements, atmospheric turbulence and weather. It is not always possible to locate a ground station on the highest peaks or in the best areas for year-round weather, which means that the beam quality from the ground site will always fluctuate. Due to advances in astronomy and imaging, adaptive optics is now considered the preferred method of severely reducing aberration in the laser beam limiting the spread of the beam as it traverses the atmosphere.

This "cleansing of the beam" is accomplished by using an optical element such as a mirror to reverse the phase aberration of the light beam. The mirror is comprised of many different elements, or smaller reflecting surfaces, which are individually changed through a feedback system run by a computer. The computer samples the incoming light and reverses the phase. It then sums the phase aberration from the mirror with the new incoming light forcing the phase to go to zero and leaving the outgoing beam planar. This requires a sampling light, ideally a laser onboard the satellite which is receiving the beam. This sampling light is directed back along the laser path, and is then used as the basis for reversing the phase of the original signal.

Using adaptive optics in laser communications is a very delicate science and has specific power and pointing requirements, especially since the satellite is traveling at a velocity which changes the time required for the beam to reach the satellite and then be directed back down. As an added difficulty, most satellites do not carry an onboard laser to use as sampling signal which means an alternate light source with its own error sources must be created.

Even though this type of system is still in the developmental stages in most places, its applications could be endless. Communications technology improves radically every few years, and with the help of adaptive optics, the next big leap could be right around the corner.

B. ADAPTIVE OPTICS IN OTHER APPLICATIONS

1. Medicine

Communications and astronomy are not the only area that uses adaptive optics. In recent years the medical community has been using it in the field of ophthalmology. In much the same way that astronomers use adaptive optics to remove aberrations from images, doctors are now using it to cancel out imperfections in the eye in a procedure known as LASIK surgery. Doctors can now detect the smallest imperfections in the eye by directing a planar wave into the eye and analyzing the returned wavefront (McMahon). The difference in the waves will show any flaw that is characterized in the eye. This data can now be used to improve eyesight even in what was once thought of as "perfect vision". Before the advent of adaptive optics, doctors were only able to address problems with astigmatism and defocusing. Now they can detect upwards of 60 different types of imperfections, nearly eliminating the need for lengthy analysis using lenses and microscopes.

Correcting these imperfections also involves the use of adaptive optics. The information gathered from analyzing the wavefronts is used in a procedure known as LASIK or Laser In-Situ Keratomileusis. LASIK surgery permanently alters the shape of the cornea with very few side effects or pain. Using the data from the analysis the laser is able to deform the cornea to match the prescription. The prescription used in this application is developed using wavefront-sensing technology. This technology is constantly evolving and it is thought by the year 2010 there will be systems in place to correct most people's vision to 20/10 (Schwiegerling).

III. FACILITIES CURRENTLY CONDUCTING WORK IN ADAPTIVE OPTICS FOR SPACE APPLICATIONS

Ground-based astronomy is limited by the atmosphere of the earth. The aberrations caused by light traveling through this mass of gases limits the areas of the heavens that can be reached by the astronomer's eye. It is also troublesome for lasers and other man-made light source traveling through it from the earth to space. This problem has recently created a demand for telescopes and laser systems that can traverse these gases cleanly creating clear pictures and uninterrupted communications. This rise in interest in space has led to a number of organizations developing systems in adaptive optics. Below are some of the major organizations that are currently conducting experiments in adaptive optics.

A. NAVAL RESEARCH LABORATORY

1. Magdalena Mountain Project

The Naval Research Lab is currently working on a project to be completed in 2006 in the Magdalena Mountains, located in central New Mexico, to create an optical interferometer aimed at increasing sensitivity for ground-based interferometry systems. To do this, they are experimenting with how adaptive optics systems combined with medium-sized optical apertures will redefine the way star positions are measured.

The technology used at the Magdalena Ridge Observatory is based on the research done at Navy Prototype Optical Interferometer (NPOI). By combining the results of the NPOI study (a high-precision, long baseline optical interferometer that allows star position measurements to very accurate detail) with adaptive optics, the NRL hopes to enable the use of medium-sized telescopes for deep-space imaging by increasing the sensitivity of the telescopes. By linking several medium sized telescopes together through interferometry, a higher resolution signal is produced. Adaptive optics will make the signal even crisper. Such systems will be used to study far-off star and solar systems and when decoupled can be used for satellite tracking and imagery in our own planetary system.

2. Portable Adaptive Optics

Working out of a laboratory in Albuquerque, NM, the Naval Research Laboratory has designed a portable adaptive optics system. This system, one of the most compact of its kind, is lightweight and can be used in combination with most telescope systems. The system has been successfully tested on the Kitt Peak 1.3 meter telescope at Kitt Peak, Arizona.

By building a portable system with a smaller footprint, researchers are not confined to one telescope on one system. This also reduces overall system cost by using lower-power systems that still have the capability for wavefront sensing and correction. Part of the NRL's objective with these systems is to implement alternative computer components for deformable and tip/tilt mirror control in an effort to cut cost, weigh and power consumption without losing capability.

B. KECK OBSERVATORY

In December of 2001, Keck Observatory in Hawaii launched its Laser Guide Star program, the largest of its kind, on its 10 meter Keck II telescope combining the powerful Keck II optics with a state of the art laser guide star adaptive optics system. Keck, in collaboration with Lawrence Livermore National Laboratory, developed the high-speed wavefront control system and the laser system along with the opto-mechanical system, user interface, and control system. This system is based on a 349 acutator continuous surface deformable mirror coupled with a Shack-Hartmann wavefront sensor and a 589nm pulsed solid-state-pumped dye laser. The "first-light" ceremony held December 23 2001 (Center for Adaptive Optics) was a complete success and is now in full operation used for both education and research.

The laser guide star system, which is based on flash-pumped solid state Nd-Yag lasers, is one of the few of its kind in the world. Its wavefront sensor is a Shack-Hartmann sensor with 241 subapertures arranged in a square pattern in order to match up with the actuators in the deformable mirror built by Xinetics. A second sensor was built into the system and used when the laser guide star is in operation (LLNL).

C. AIR FORCE RESEARCH LABORATORY

For the last few years the AFRL has been researching adaptive optics techniques for use in free space optical communications. The goal of this type of research is to provide improvement in ground-to-ground, ground-to-air, and air-to-air communications links. Current research has been able to increase system bandwidths to greater than 6Khz up to 10Khz (NEPAC,1).

Free space optics uses light beams in the non-visible range to provide optical bandwidth connections. It is used for sending data, voice and video communications simultaneously through the atmosphere, with a connectivity similar to fiber optics without the cable, enabling optical communications at the speed of light. FSO works on line-of-sight technology, allowing travel through the air much faster than any other medium. Combining this technology with adaptive optics can lead to communications that are faster and crisper at a much longer distance. By eliminating the deformations caused by atmospheric turbulence it could be possible to design such systems in the future for ground-to-space communications.

1. Starfire Optical Range

The Starfire Optical Range (SOR) is considered by many to be one of the premier adaptive optics research centers. Their primary focus is to develop control technologies for wavefront sensing and correction. The SOR boasts a 3.5 meter telescope for satellite tracking, a 1.5 meter telescope, and a 1 meter beam director.

Figure 2. Starfire Optical Range Albuquerque, NM[3]

Among their many research endeavors in adaptive optics, SOR had successfully developed an AO system for their 1.5 meter telescope capable of using lasers as artificial beacons in order to sense aberrations. Normally, bright stars would be used for this, but doing it artificially allows it to cover a greater area of interest. This allows research in areas of the sky previously unattainable due to the lack of natural bright stars.

SOR is unique in its adaptation of technology surrounding the 3.5 meter telescope. By combining adaptive optics with the use of a sodium wavelength laser beacon, it is hoped that near diffraction limited performance can be achieved, giving SOR the ability to obtain ultra-high resolution images at visible wavelengths. The system itself consists of a fully collapsible classical Cassegrainian optical telescope that uses a coudé path and is cooled by a state-of-the-art closed-cycle water system. In September of 1997, SOR was able to begin taking images with the AO system. By putting an emphasis on minimizing thermally-induced turbulence at the facility, SOR was able to obtain high-quality images such as the one shown below.

[3] "View of SOR Taken From Helicopter." No Date. Online Image. Starfire Optical Range Facilities. 30 October 2005. <http://www.afrl.af.mil/images/pictures/sor-aeri.jpg>

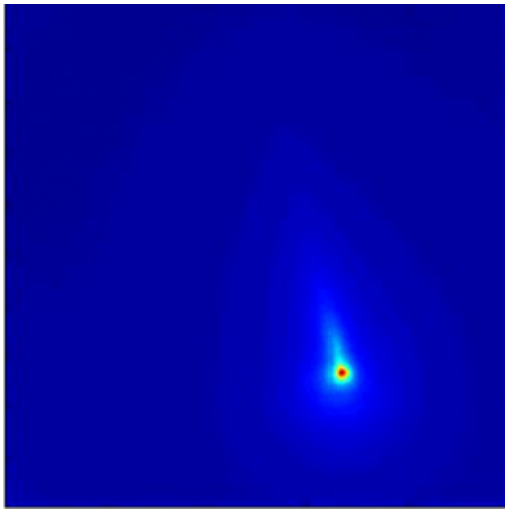

Figure 3. Close up of the head of the Hyakutake Comet taken with the 3.5m telescope[4]

Another area of study at SOR is active imaging. The Active Imaging Test bed, finished in 1999 was designed to acquire imagery of low-earth satellites. By using a camera mounted on the large 3.5 meter telescope, SOR was able to demonstrate the acquisition, tracking and illumination of LEO satellites using high quality laser beams. Data from the camera was processed to produce images of the satellites.

These are only some of the many projects underway at the AFRL. Through the use of adaptive optics, laser systems, and optical communications research, the AFRL is leading the way toward the development space-based technology and high-quality space imagery.

[4] "Hyakutake Comet." 23 March 2005. Online Image. Starfire Optical Range. 30 October 2005 <http://www.de.afrl.af.mil/SOR/comet.htm>

THIS PAGE INTENTIONALLY LEFT BLANK

IV. THE PHYSICS OF OPTICS

A. PROPERTIES OF LIGHT AND WAVES

Light, also known as electromagnetic radiation, can be interpreted as a wave in an electromagnetic field, as a stream of photons, or as small packets of particles. In his Treatise of Light, Huygen described light as traveling in a wave motion, spreading out from its source in all directions to propagate through the atmosphere. Simply put, light travels in a wave as seen in the picture below.

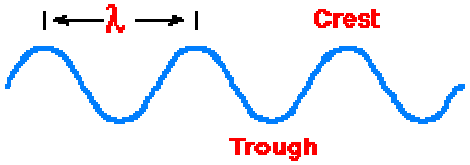

Figure 4. Formation of a wave[5]

This wave, as with waves in water or sound, has an associated wavelength most commonly described with the Greek letter lambda (λ). As light propagates through a medium, it travels at a certain speed depending on the composition of the medium it is traversing. In a vacuum, it will travel at a speed known as the speed of light designated as ($c = 3 \bullet 10^8 m/s$).

Sir Isaac Newton, a contemporary of Christian Huygen, expounded on Huygen's theories on light propagation and wave theory. Huygen developed laws depicting the characteristics of reflection and refraction of light in different medium. A few years later, Newton published his papers called Optiks which describes in detail how light propagates. Specifically, he describes the tracing of rays which becomes important in geometric optics. It wasn't until the early 1900s that Einstein would take Newton's ideas and Huygen's principles and reconcile them to explain the photoelectric effect.

In the late 1800s, Thomas Maxwell developed his equations, known as Maxwell's Equations, which would be used to describe the properties of an electromagnetic wave,

5 "Light as a Wave." No Date. Online Image. Wave Properties of Light. 04 October 2005 <http://csep10.phys.utk.edu/astr162/lect/light/waves.html>

which in turn described light as a part of the electromagnetic spectrum. This breakthrough in science changed how the propagation of light was studied.

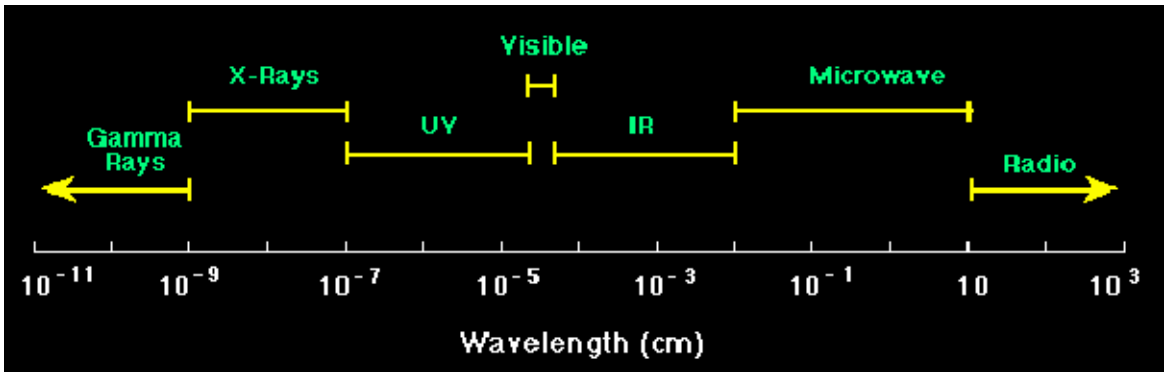

Figure 5. Electromagnetic Spectrum[6]

Maxwell's equations were quantized as:

$$\nabla \bullet \vec{B} = 0 \quad B = magnetic\ field$$

$$\nabla \times \vec{E} + \partial \vec{B} / \partial t = 0 \quad E = electric\ field$$

$$\nabla \bullet \vec{D} = \rho \quad D = electric\ displacement, \rho = density\ of\ the\ electric\ charge$$

$$\nabla \times \vec{H} - \partial \vec{D} / \partial t = \vec{J} \quad J = current\ density, H = magnetic\ field\ strength$$

$$where\ D = \varepsilon_o \vec{E} + \vec{P}, \varepsilon_o\ is\ the\ permittivity\ of\ free\ space, and\ P\ is\ the\ polariztion$$

In the early 1900's, Max Plank was able to take these early theories and describe them as quantum energy, better known as the study of quantum mechanics. Just as a wave is described with its wavelength, it can also be characterized by its frequency (*f*). The frequency is the number of wavelengths that pass through a fixed point in a fixed period of time. In equation form $f = cycles / time\ (1/s)$. Plank described this in reference to the energy of a quantum of electromagnetic radiation. According to him, this electromagnetic radiation is proportional to the frequency of that radiation called "nu" (υ).

$$E = h\upsilon = \frac{hc}{\lambda}$$

6 "The Electronic Spectrum." No Date. Online Image. The Electromagnetic Spectrum. 6 October 2005. <http://csep10.phys.utk.edu/astr162/lect/light/spectrum.html >

In the above equation h is known as plank's constant equal to $6.63 \bullet 10^{-34} Js$.

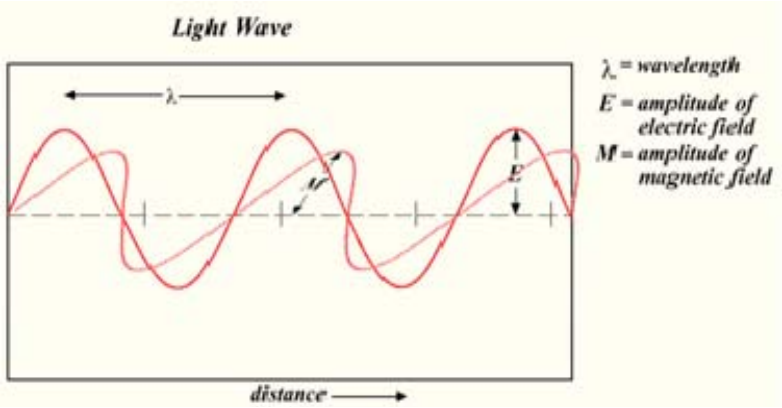

Figure 6. Light propagation as a function of electric and magnetic fields[7]

In 1924, de Broglie suggested that subatomic particles have a wavelength which has the characteristic of momentum (p) $\lambda = h / p$. This cemented the idea that light could be seen both as a wave and as a particle. This wave-particle duality is used to more adequately explain how light travels and interacts with other particles on a quantum level. Quantum mechanics describes both light and matter. Using wavelength and momentum, material particles such as electrons and neutrons and photons (packets of light) are described using these equations:

$$p^2 = \frac{E^2 - m^2c^4}{c^2}, \textit{ and combining this with the wavelength equation,}$$

$$\lambda = \frac{h}{p} = \frac{hc}{\sqrt{E^2 - m^2c^4}}, h\upsilon = \frac{hc}{\lambda} \quad (m = \textit{mass at rest})$$

$$\therefore \ \upsilon = \frac{pc^2}{E} = c\sqrt{1 - \frac{m^2c^4}{E^2}}$$

For photons, which are without mass, these equations simplify to

$$p = \frac{E}{c}, \ \lambda = \frac{h}{p} = \frac{hc}{E}, \ \upsilon = \frac{pc^2}{E} = c$$

[7] Heron. "Light Wave." 26 June 2004. Online Image. Wikipedia: Electromagnetic Spectrum. 6 October 2005. <http://en.wikipedia.org/wiki/Electromagnetic_radiation >

B. BASIC OPTICAL CONCEPTS

1. Reflection

Reflection occurs when light is buffeted off of a surface instead of traveling through it. This happens according to the law of reflection. A ray of light is incident on a surface at an angle to the normal known as the angle of incidence (θ_i). When this ray of light is reflected off of the surface, the angle the reflected ray makes with the normal is called the angle of reflection (θ_r). These two angles are always equal to each other for a ray of light reflecting off of a planar surface $((\theta_i = \theta_r)$.

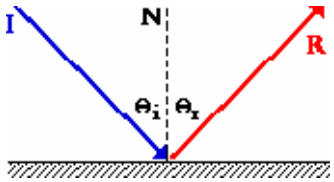

Figure 7. Reflected ray of light[8]

a Real Image

A real image is a representation of a physical object formed by an optical instrument. A real image is produced when rays of light pass through the image and are brought to focus at the image position. If a screen or white paper is placed in the plane of a real image, it will become visible. An example of a real image is a picture on a piece of paper.

b. Virtual Image

A virtual image is an image that appears to be at a different position from where the light was reflected as with a reflection in a mirror. The image appears to be in the plane of the mirror, but the physical object and the light reflecting from that object are actually being reflected in front of the surface of the mirror.

2. Refraction (Snell's Law)

Refraction occurs when the speed of a ray of light changes as it passes from one medium to another. This change in speed causes the ray to bend, or refract. The degree to which the ray bends is called the index of refraction denoted with n_r. Every medium,

[8] Henderson, Tom. "Reflection." 2004. Online Image. The Physics Classroom. 8 October 2005. <http://www.glenbrook.k12.il.us/gbssci/phys/Class/refln/u13l1c.html>

including air, has an index of refraction ($n_{air} = 1$). The angle of refraction is the angle the ray of light makes normal to the new medium.

Snell's law shows the relationships between the incidence angle, the angle of refraction, and the indicies of refraction. Snell's law states that $n_1 \sin(\theta_1) = n_2 \sin(\theta_2)$.

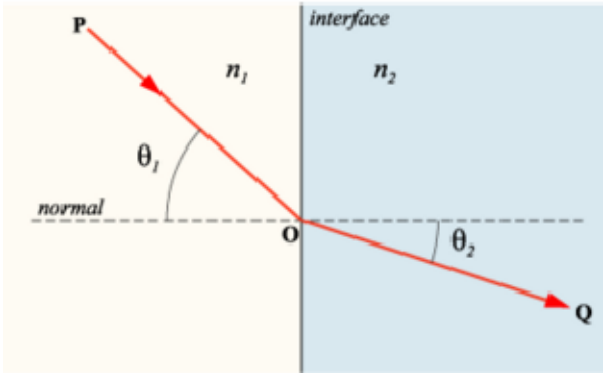

Figure 8. Depiction of Snell's Law[9]

a Total Internal Reflection

Total internal reflection occurs when a ray travels from a medium of higher refractive index to a medium of lower refractive index at an exit angle that is greater than the incident angle. The ray is no longer refracted, but completely reflected back into the medium of higher refractive index at an angle equal to the incident angle. When the refraction angle becomes 90^o to the normal, the critical angle, or the angle at which the refraction becomes a reflection, can be found $n_1 \sin(\theta_c) = n_2 \sin(90^o)$.

3. Diffraction

Huygen's principle states that all points along a wavefront act as if they were point sources. When a wave encounters an obstruction with a small slit or hole, all but a few of these points along the wavefront are blocked. Those that come through the slit will not continue on their original path, but will move in all different directions. This bending of light is called diffraction. Diffraction is seen in all kinds of waves including sound waves, water waves, and electromagnetic waves. Diffraction can occur in groups

[9] Wikipedia. "Reflection of Light at the Interface Between Two Media of Different Refractive Indicies." No Date. Online Image. Wikipedia: Reflection. 8 October 2005. <http://www.answers.com /topic/snell-s-law>

of waves of a finite size, such as light coming from a flashlight or a laser beam, causing the beam of light to become larger and larger as it moves away from its source.

When the width of the opening through which the wave is passing is of the same order or less than the wavelength of light being used, the diffraction effects become very noticeable. An image can appear to be distorted when light diffracts around the object due to object being smaller than the wavelength of the light being used to illuminate it. This is called diffraction limited, meaning that the diffraction limits the power or effectiveness of the imaging aperture. When examining the light coming through a slit, it is intuitive that the properties of the slit system depend on the wavelength of the light and the width of the slit given in the ratio λ / w. The intensity of the light on the outgoing side of the slit creates a pattern of dark and bright fringes. The dark fringes occur at an angle that can be described by the relation $\sin\theta = (m\lambda)/w$ where m=1,2,3… An image can be in the near field or the far field which dictates the type of diffraction that will occur.

a. Near Field vs Far Field

The near field is generally understood as that part of the radiated energy field that is no further away than a quarter wavelength of the diffraction edge or the region that is close to the aperture. The near field is generally much closer than a quarter wavelength, and anything beyond a quarter wavelength is considered diffraction limited. This concept of near field is not quite as simple as this, although a quarter wavelength is considered accpetable in some research areas. A point called the Raleigh range delineates the distance at which the near field approximation is no longer valid. The Raleigh range is the distance from the beam waist at which the curvature of the wavefront is at its maximum. The diffraction pattern for the near field will differ significantly from that of the far field. The far-field region is considered to be infinity (or greater than $2d^2/\lambda$ from the source) when the diameter of the beam (d) is large compared to the wavelength. Light focused at infinity is said to be in the Fraunhofer region, otherwise known as the far field. The Fraunhofer region is where the diffraction of the light through an aperture for small values of the Fresnel number occur (F <<1). The Fresnel number is defined as $F = r^2/d_a\lambda$ where r is the distance from the aperture to the screen

and d is the diameter of the aperture. Collimated or plane wavefronts are considered to be in the far field because the light source and observation position are far from the diffraction aperture (pinhole or slit). In near-field or Fresnel diffraction, the curvature of the wavefronts has to be taken into account due to the close approximation to the diffraction aperture. When the observation screen is moved in relation to the aperture, far field patterns will change uniformly in size, whereas the near-field patterns changes will vary in size and shape.

4. Lenses

There are many types of lenses made today, the most common of which are spherical lenses. Spherical lenses can be concave or convex in nature. A convex lens is one in which the lens is rounded outwardly and the radius is positive. A concave lens protrudes inward and its radius is considered to be negative. If a lens is neither concave nor convex it is said to be planar or flat.

A lens is characterized by its focal length which is the point at which all parallel rays coming through the lens will be focused. The inverse of the focal length is defined as the strength of the lens. The focal length can be found by using the lensmaker's formula:

$$\frac{1}{f} = \frac{n_2 - n_1}{n_1}\left(\frac{1}{R_1} - \frac{1}{R_2}\right)$$

$$f = \textit{focal length}, n_1 = \textit{refractive index of surrounding medium}$$

$$n_2 = \textit{refractive index of lens}, R_1 \,\&\, R_2 = \textit{radii of curvature of the two surfaces of the lens}$$

When working with thin lenses in air (n=1) the lensmaker's formula reduces to

$$\frac{1}{f} = \frac{1}{s} + \frac{1}{s'}$$

$$s = \textit{distance to the image}$$

$$s' = \textit{distance to the object}$$

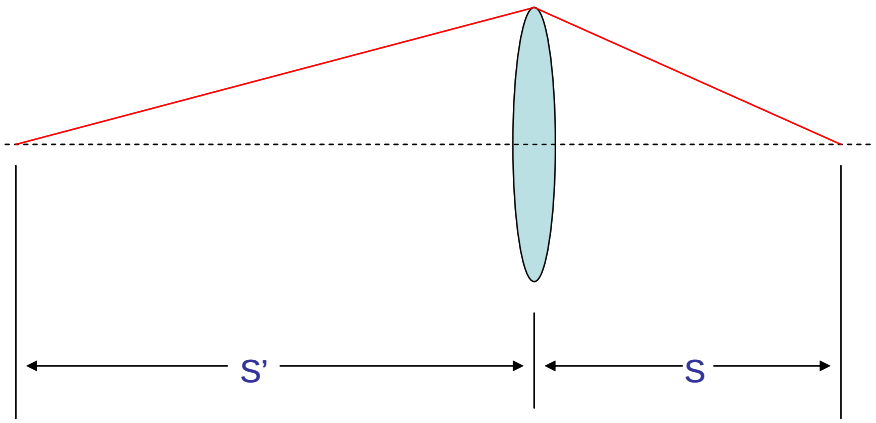

Figure 9. Lens maker's formula for a thin lens

The magnification of the lens is m=s/s'.

Lenses are commonly manufactured as singlets and doublets. Singlets are just that, a single lens. Singlets are limited by the aberrations inherent in the lens. Doublets are two lenses manufactured as one. Achromatic doublets are limited by diffraction and are preferred by those who work with advanced optical systems. They consist of a convex lens and a concave lens of different glasses that have been cemented together, producing a compound lens that has a larger focal length.

a. Sign Conventions

The radius of curvature of the lens will dictate the sign of the lens. For the front surface of a lens, a concave lens' radius is considered to be positive and for a convex lens the radius is considered to be negative. The back surface of the lens is reversed so that if it is concave it is positive and if it is convex it is negative. The area above the axis is considered positive and below the axis negative.

5. Lens Combinations

For complex optical systems, lenses can be combined to achieve desired effects. Each lens has a distinct focal length and when used together the focal lengths determine the distances to which the lenses will be effective. When using a combination of thin lenses, the combined focal length of the system can be found by $\frac{1}{F}=\frac{1}{f_1}+\frac{1}{f_2}$. The

combined power of the lens is simply P_1+P_2 for lenses that are not separated. For lenses separated by some distance (d), the equation for power becomes $P = P_1 + P_2 - P_1 P_2 d$.

6. Lens Aberrations

a. Coma

Coma is an aberration that is off-axial and non-symmetric about the optical axis, causing it to be unable to focus at a particular point instead creating a fuzzy circle. It is called coma because it takes on a comet-like look the further off the axis it gets. It is possible for a lens with a large coma to create a very sharp image with considerable blurring toward the edges of the image. Coma can sometimes be corrected by simply bending the lens, but it is more effective to use a combination of lenses to correct it.

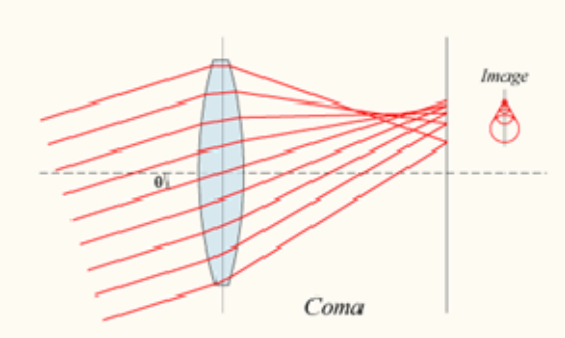

Figure 10. Example of Coma[10]

b. Distortion

Distortion occurs when the image geometrically differs from the object. Distortion can be negative or positive depending on the variation in the magnification or the power of the lens. Every lens imparts some level of distortion to an image. When there is no distortion, the image is crisp and appears exactly like the object imaged. Negative distortion causes the image to "barrel" or bulge out in the center. Positive distortion causes the image to push in, giving pincushion effect, as if the image is being

10 "Diagram of a Coma Aberration in a Lens." No Date. Online Image. Wikipedia: Lens (Optics). 2 Nov 05. <http://en.wikipedia.org/wiki/Lens_(optics)>

squeezed simultaneously on all four sides. To avoid this effect, the effective diameter of the lens should be as small as possible.

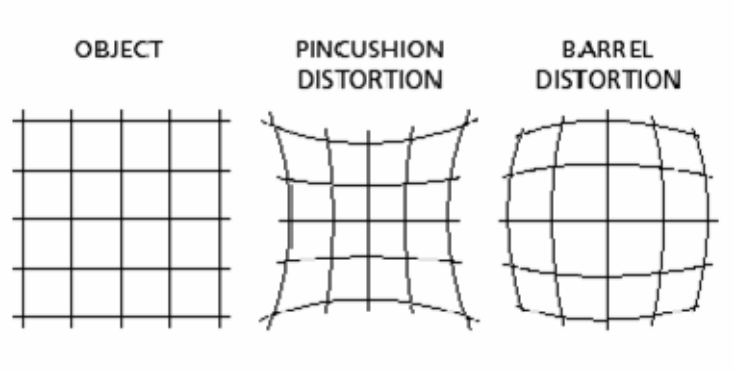

Figure 11. Effects of Distortion[11]

c. Defocus

Defocus is so easily fixed that it is not generally considered an aberration. Defocus is a first order aberration and will vary as the distance to the center of the lens varies. Defocusing of the lens will cause the image to blow up in a blur or distort smaller and smaller, depending on whether it is inside focus or outside focus. This is easily fixed by moving the lens along its center axis until the image sharpens. This will be discussed more in Chapter VI.

d. Astigmatism

An irregularity or asymmetry in the curvature of a lens can cause an aberration called astigmatism. Astigmatism causes the image to spread along the axis as if being pulled from opposite sides. It will also appear to be out of focus. Lenses with astigmatism will have different focal lengths for the different rays of light entering the lens off its central axis.

[11] "Diffraction." No Date. Online Image. Optics-Online. 4 Nov 2005 <http://www.cartage.org.lb/en/themes/Sciences/Physics/Optics/Optical/Lens/Lens.htm >

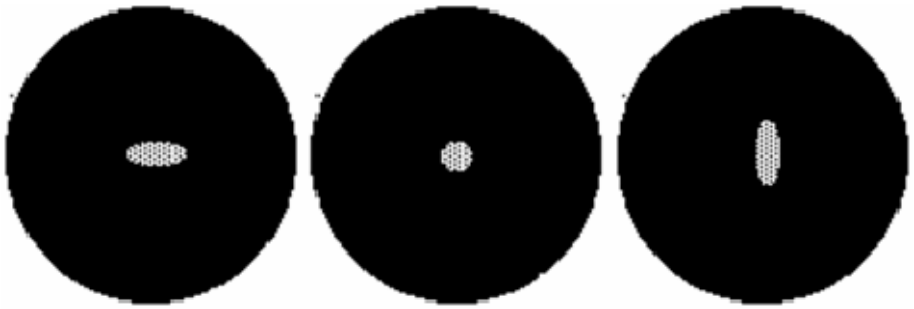

Figure 12. Astigmatism aberration, from left to right : inside focus, best focus, outside focus[12]

The use of multiple optical elements can significantly reduce astigmatism.

e. Spherical Aberrations

Spherical aberrations are characteristics of spherical lenses (singlets, or lenses that are not combined with other lenses) and mirrors. This type of aberration causes parallel rays of light striking the lens at different distances from the optical axis to be focused at different points along the axis. With spherical aberrations, one of two things will generally happen. Either the Airy disc will disappear and a fuzzy bright fringe will appear, or the inner diffraction ring will be extraordinarily bright causing the Airy disc to blend with the inner fringes. Spherical aberration can be corrected to some extent by choosing particular lenses for specific purposes such as using plano-convex lens to focus a collimated beam. With the convex side toward the beam, the focal point will appear sharper and reduce the aberration. Because of the nature of lenses that are combined (doublets), these lenses will not produce any spherical aberrations in themselves and are often used for this reason in optical systems.

[12] "Astigmatism Aberration, From Left to Right: Inside Focus, Best Focus, Outside Focus." No Date. Online Image. Virtual Newton Telescope. 4 Nov 2005 <http://www.cg.tuwien.ac.at/studentwork/CESCG/CESCG99/AGascon/ >

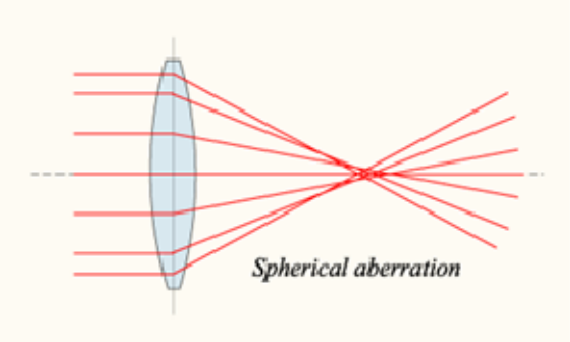

Figure 13. Spherical Aberration

Spherical aberration in a lens can be given by the relation (Pedrotti and Pedrotti, 95)

$$\frac{1}{s_h'}-\frac{1}{s_p'}=\frac{h^2}{8f^3n(n-1)}\left[\frac{n+2}{n-1}\sigma^2+4(n+1)\left(\frac{s'-s}{s'+s}\right)\sigma+(3n+2)(n-1)\left(\frac{s'-s}{s'+s}\right)^2+\frac{n^3}{n-1}\right]$$

$$s_h = image\ distance\ for\ a\ ray\ at\ elevation\ h,\ \ s_p = paraxial\ image\ distane$$

$$s' = image\ distance,\ \ s = object\ distance$$

$$\sigma = shape\ \ factor,\ \ n = index\ of\ \ refraction$$

$$f = focal\ length$$

C. THE LASER BEAM

A laser beam is normally referenced to by its brightness a measure of the output power of the laser as a function of its propagation distance. By dividing the brightness on a star by the square of the distance from the beam aperture to the star the energy density can be found. Brightness is be expressed as a function of the Strehl ratio (S) (see Chapter VI), thermal and fluxuation effects (α), temperature (T), shape (z) and diameter (D) of the aperture, and the wavelength (λ).

$$B=\frac{TD^2P(x)\pi Sz}{4\lambda^2\left[1+\left(\frac{2.22\alpha D}{\lambda}\right)^2\right]}\left[\frac{Watts}{steradian}\right]\qquad \rho = B/\sqrt{d}$$

The intensity of the beam can be expressed as a function of the distance it propagates (x) as shown by the formula below.

$$I_o = \frac{(D/2)^4 \pi^2}{(\lambda x)^2} I_a, \quad x >> D$$

$$I_a = intensity\ at\ the\ aperture\ (W/m^2)$$

When taking into consideration aberration, this equation becomes:

$$I_o = \frac{S(D/2)^4 \pi^2}{(\lambda L)^2} I_a, \quad S = Strehl\ Ratio$$

The output aperture of the laser beam is generally uniformly circular in shape (z=1), creating a cylindrical shaped beam which propagates through a certain distance x. A Gaussian beam takes on the form shown in the picture below.

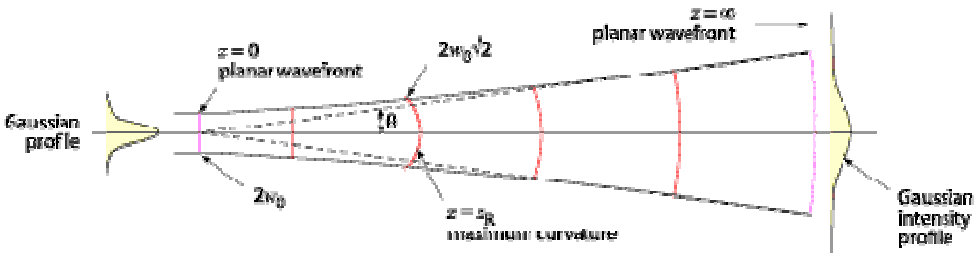

Figure 14. Profile of a Gaussian Beam[13]

Several important parameters of the Gaussian beam are the beam waist, beam size, beam radius, and spot size. The circular profile of the beam as it leaves the output aperture of the laser is the beam diameter. The Gaussian beam is most intense at its center point known as the beam waist (z=0). As the beam travels along the axis, the diameter of the beam changes according to distance. The value at which the power per unit area of the beam becomes 1/e of the value at the waist is called the spot size, q. Both the radius of the beam and the spot size will increase as the distance from the beam waist increases.

[13] Melles Griot, Inc. "Changes in Wavefront Radius with Propagation Distance." 2002. Online Image. Gaussian Beam Propagation. 10 November 2005. http://www.mellesgriot.com/products/optics/gb_2_1.htm

THIS PAGE INTENTIONALLY LEFT BLANK

V. TEST BED COMPONENTS

Several important pieces of equipment were used to construct the Adaptive Optics test bed. The main optical components are a laser, spatial filter, fast steering mirror, deformable mirror, and a wavefront sensor. To simplify the design, the fast steering mirror was put aside for future use. It is important to understand each device and what its function is, so they are listed here.

A. LASER

The laser being used is a 532nm diode-pumped green laser manufactured by B&W Tech. The laser is a self-contained, thermally controlled, frequency doubled Nd:YV04 laser that produces a stable output power of 50mW. This laser produces and excellent beam mode quality and low divergence which makes it suitable for signal transmission and long-distance positioning.

Figure 15. B&W Tech 532nm green laser

B. SPATIAL FILTER

Spatial filters are used in optical systems to clean up the beam. The aberration in the beam can come from many places such as a poor quality laser or dust on the optic. This causes blurry spots, asymmetrical beams, or concentric rings appearing around the center spot of light (caused mostly by the diffraction of the light off of the dust particles).

The way a spatial filter works is to use a focusing lens with a short focal length such as the microscope objective (8mm) in conjunction with a pin hole (in this case approximately $5\mu m$). The objective is to focus the laser beam to a spot, placing the pinhole at the focal point, which forces the light directly through the hole. Collimating the light forces the beam to behave as if it was generated by a distant point source. The lens does a Fourier transformation, with the pinhole minimizing the frequency spectrum of the wavelength by selecting the lower frequencies. In other words, the microscope objective produces a diffraction pattern constituting a Fourier transformation of the light from the object plane. The spatial frequency constitutes the diffraction pattern of the object. This means that the spatial frequency is proportional to the distance from the axis of the system. The pinhole eliminates the high spatial frequencies, letting the low-frequency parts of the beam profile pass through the pinhole. This is in effect a smoothing of the beam. The Fourier transformation is reversed by the output (collimating) lens and the light expands as it comes out of the pinhole. This eliminates the intensity variations from the beam and projects a filtered diffraction pattern, which when seen through a shear plate will result in straight dark fringes.

The fraction of power that passes through the pinhole can be found by:

$$P_f = 1 - e^{-\frac{1}{2}\left(\frac{\pi r D}{\lambda F}\right)^2}, \quad P_f = \frac{Power\ out}{total\ \ power}$$

$$r = radius\ of\ \ the\ beam$$

$$D = diameter\ of\ \ the\ \ pinhole$$

$$F = focal\ length\ of\ \ the\ microscope\ objective$$

The optimum diameter of the pinhole is found to be $D_{opt} = (F\lambda)/r$. The minimum wavelength of noise that will pass through the pinhole can be found by $\lambda_{n(\min)} = (2F\lambda)/D$.

Positioning the pinhole requires precision measurement which needs to be done with an xyz micrometer translator. The pinhole is only accurate to $\pm 1\mu m$ and needs to be positioned in the exact place so that the focal length of the lens meets the focal length of the microscope objective.

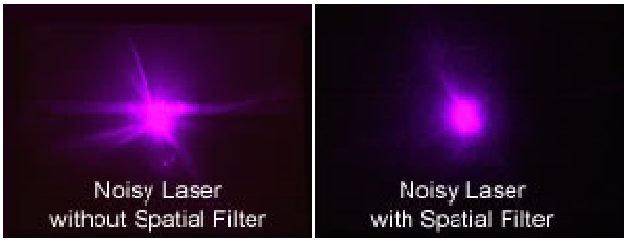

Figure 16. Example of Spatial Filtering With a Laser[14]

C. DEFORMABLE MIRROR

Micromachined deformable mirrors (MMDMs) are composed of many different elements. Each element is controlled by a voltage which is varied to deform the mirror. The mirror being used was developed by OKO Industries and has 37 elements. This mirror was chosen due to its ability to correct low-order optical aberrations. The voltage applied to each element is unique to that element. When all of the elements are used in conjunction with each other the aberration or deformation detected by the wavefront sensor is corrected and a perfectly planar wave is created.

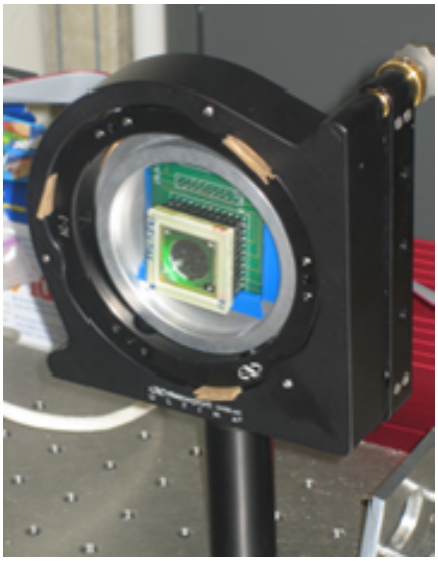

Figure 17. MMDM

Micromachined deformable mirrors (MMDM) are manufactured using cutting edge processing technology. Silicon chips are micromachined in bulk, mounted to a

[14] StockerYale, Inc. "Spatial Filter." 2005. Online Image. 30 October 2005. StockerYale: Glossary. <http://www. stockeryale.com/i/lasers/glossary.htm>

printed circuit board holder, and coated to form a reflective surface. The mirror package, which is a part of the printed circuit board, contains the control electrode and other electronic components. Voltages applied to these components control the reflective membrane and shape of the mirror.

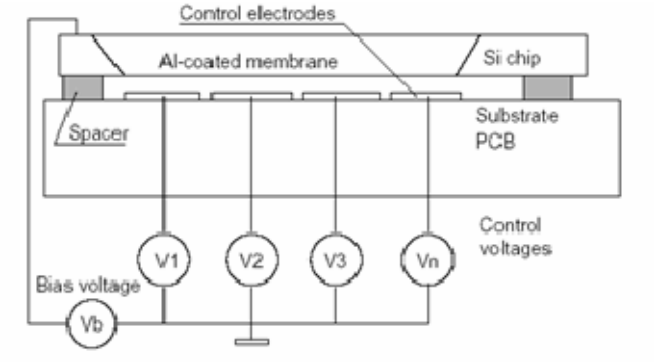

Figure 18. Schematic of the Deformable Mirror[15]

D. PIEZO-ELECTRIC MIRROR

Even though the piezo-electric mirror was not initially designed into the test bed, it will be discussed here because it will become an integral part of the design in the future. The mirror is very similar in operation to the MMDM. It consists of 19 column-like actuators that are bonded to the base. Each actuator is mounted with a reflective plate that is coated to create a mirror. The face of the mirror is controlled by voltages that are applied to each individual actuator. The mirror being used was manufactured by OKO Industries.

The piezo-electric mirror will be placed in the system prior to the deformable mirror and used to induce aberrations into the system, which will be corrected by the MMDM.

E. WAVEFRONT SENSOR

The wavefront sensor being used is a Shack-Hartmann sensor, manufactured by OKO Technologies which uses a Basler A601f camera. This sensor was designed to be used with the deformable mirrors also purchased from OKO Technologies.

[15] "Schematic of Deformable Mirror." 2003. Image from document. 37(19) Channel Micromachined Deformable Mirror System: Technical Passport. Delft, The Netherlands: OKO Technologies, 2003.

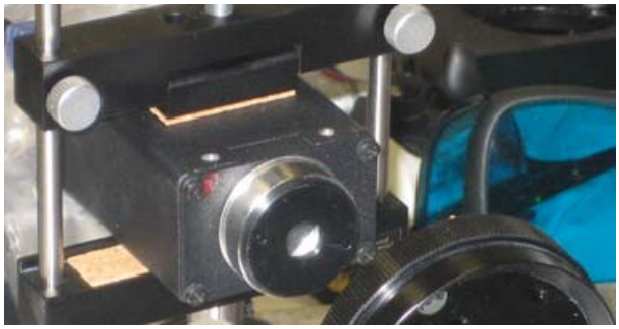

Figure 19. Shack-Hartmann wavefront sensor manufactured by OKO Technologies with a Basler CCD.

The Basler WFS has 322096 pixels arranged with 656 horizontal and 491 vertical. The camera features include adjustable brightness and gain with the highest gain available of 12 dB.

There are 127 microlenses in a hexagonal arrangement with a pitch of $300\mu m$ and a focal length of 15mm for each microlens. A linear reconstructor is used with the wavefront sensor, in this case it is written into the FrontSurfer program. The reconstructor converts the signals from the sensor into phase aberrations using a singular value decomposition matrix method.

1. Principles of Operation

The purpose of the Shack-Hartmann sensor is to measure the slope of a wavefront. This device works by using its sensor to sample a small portion of the wavefront from the light source or laser.

A Shack-Hartmann sensor is arranged in a quadcell structure. A quadcell is a grouping of four pixels in a grid formation. The quadcell array in the Shack-Hartmann wavefront sensor is made up of many of theses pixel grids.

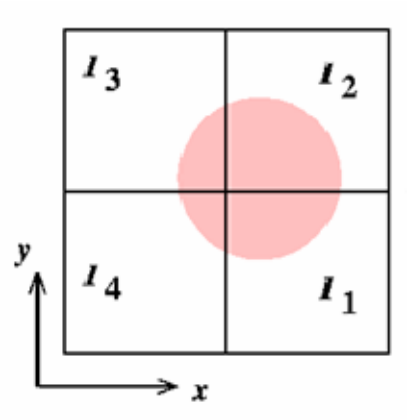

Figure 20. Shack -Hartmann Grid Formation[16]

The wavefront impinges on the quadcell and is focused on the center of the four pixels. Any light that is not normal to the center of the pixel grid is displaced toward other adjacent grids. The difference or shift in movement from where the light source impinges on the pixels is the gradient or slope of the incoming light source.

When used with a telescope system an incoming image or light source is projected onto a series of lenses called a lenslet array. These lenses are identical and have a small focal point (in our case 15mm). The lenses in the array re-form the image or light source previously taken by using sub-pupil or small sections of the aperture.

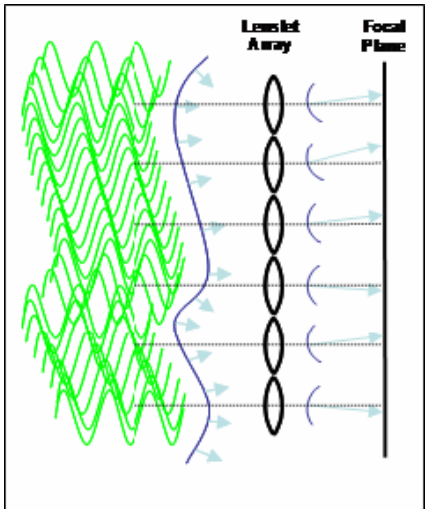

Figure 21. Shack Hartman lenslet array with impinging non-planar wave[17].

16 "Quad-cell Formation." No Date. Online Image. Wavefront Sensors: Requirements to Wavefront Sensing. 12 October 2005. < http://www.ctio.noao.edu/~atokovin/tutorial/part3/wfs.html>

The incoming collimated light source is a plane wave. This wavefront is then distorted by an artificial disturbance. The impinging light or image is then shifted from its original (normal) position on the quadcells.

By calculating the difference between the quadcells, the slope of the wavefront can be measured. This is done continuously using a lenslet array in front of the quadcell array. The distribution of light is constantly sampled by the camera and read out to the computer. The displacement of the center of the wave in the x and y directions is proportional to the average slope of x and y in the subpupils. The slopes of the light changes over time are calculated by adding and subtracting the light seen by the quadcell. The result is the calculated orthogonal slope of the wavelength. The wavefront is reconstructed from the measured slopes. Because the lenses on the wavefront sensor are completely achromatic (a color without an identifiable hue, i.e. black, white, grey or brown) the calculated slopes are not dependant on the wavelength of the incoming light.

To accurately compute the centroid there needs to be many samples taken using the quadcells. In a quadcell, the slopes are calculated by using intensity ratios taken from each pixel in the grid, as seen by the following formulas.

$$x \approx \frac{\alpha}{2}\frac{I_1 + I_2 - (I_3 + I_4)}{I_1 + I_2 + I_3 + I_4}, y \approx \frac{\alpha}{2}\frac{I_2 + I_3 - (I_1 + I_4)}{I_1 + I_2 + I_3 + I_4}$$

$$I = Intensity$$

This response is linear for slopes less than $\pm\frac{\alpha}{2}$ where α is the response coefficient dependant on the size of the object being imaged or the beam of the light source.

[17] Coy, Steve. "Shack-Hartmann Wavefront Sensor." 29 September 2004. Power Point Presentation: Modeling and Simulation of Beam Control Systems. MZA. 20 September 2005. <http://www.mza.com/doc/MZADEPSBCSMSC2004/ >.

THIS PAGE INTENTIONALLY LEFT BLANK

VI. USING ZERNIKE POLYNOMIALS TO DESCRIBE A WAVEFRONT

The reason for using adaptive optics is to remove aberrations from images or aberrations in laser beams caused by atmospheric aberration or seeing (the best possible angular resolution which can be achieved by a telescope when viewing within the atmosphere). The effectiveness of the adaptive optics system depends on several things including the wavelength, the aperture, the type of deformable mirror used and its sensitivity, and the quality of the source, whether it is an image or a laser light source. The return of the system is seen in its simplest form as a function of Zernike orders or Zernike polynomials.

Fritz Zernike won the Nobel Prize in physics in 1953 for his work in wavefront sensing and his invention of the phase contrast microscope. He was able to develop a set of mathematical functions to describe a wavefront. These functions came to be known as Zernike Polynomials. The Zernike functions represent specific orders of aberrations in the wavefront that correspond to certain coefficients called Zernike Coefficients. His wavefront theory is described in detail in his book "Applied Nonlinear Optics".

The wavefront is often expressed in the form of the Zernike polynomial. These orthogonal polynomials are used in defining optical systems with circular pupils. A polynomial is an expression such as a sum of powers in one or more variable multiplied by different coefficients, for example $ax^4 + bx^3 + cx^2 + dx + e$. Orthogonal polynomials are defined over a range so that $\int_a^b W(x) f(x) g(x) dx = \delta_{fg} c$ where W(x) is a weighting function and δ_{fg} is the Kronecker delta[18].

Zernike polynomials have several properties that make them useful in describing optical aberrations. They are normally defined as an infinite number of sets in polar coordinates (ρ, ϕ) where ρ ranges from 0 to 1 and ϕ ranges from 0 to 2π and are orthogonal over the interior of the unit circle, but not necessarily over independent sets

[18] Kronecker delta-δ_{ij} is defined as having the value one when $i=j$ and zero when $i \neq j$, i and j being integers.

within that unit circle. There are three components to each polynomial, radial (polynomial in nature), azimuthal (sinusoidal in nature), and radially-dependant.

The rotational symmetry is given in the form $R(\rho)G(\theta)$ where $G(\theta)$ represents the continuous function in cycles of 2π and ensures the relationship $G(\theta+\alpha)=G(\theta)G(\alpha)$ is true where α is any angle from 0-360 degrees. This means that even when rotating the coordinate system there is no change to the polynomial's form. This relationship is satisfied by $G(\theta)=e^{\pm im\theta}$ when $m=1,2,3,\ldots$. The radial function is satisfied when it is a polynomial in ρ degrees of n. In this form, it contains no power of ρ that is less than n. The radial dependency dictates that if $R(\rho)$ is even then m must be even and if $R(\rho)$ is odd then m must be odd.

In certain cases, the radial polynomials can be described in the form of Jacobi Polynomials $R_n^m(\rho)$. To eliminate the complex exponentials, the radial form of the polynomial is combined with sines and cosines. The most common form for the Zernike polynomial when being applied to wavefront sensing is written in the form of

$$\Delta W=\overline{\Delta W}+\sum_{n=1}^{\infty}\left[A_nQ_n^0(\rho)\rho^m\left(B_{nm}\cos(m\theta)+C_{nm}\sin(n\theta)\right)\right]$$

where $\overline{\Delta W}$ is the mean wavefront optical path difference (OPD) and A_n, B_{nm}, and C_{nm} are the coefficients. For a system that is symmetrical, the wavefront aberrations will appear to be symmetrical about the tangential plane and only even functions of theta will exist. However, most systems are not symmetric and both even and odd terms will appear.

Zernike polynomials are very useful because each term of the Zernike minimizes the root mean square (RMS) wavefront error to the order of that term. Each term of the Zernike is orthogonal to each lower term contained within it. The terms are structured so that adding other aberrations of lower orders will increase the RMS error, but will not cause it to degrade. As with the lower order terms, the higher order term has built into it the necessary amount of defocus and tilt to minimize RMS error to that order. Removing the first order term of defocus and tilt will represent a shift in the focal point that will maximize the intensity at that point. Shown below is a table of the existing Zernike polynomials used in wavefront analysis.

Table 1. 36 Terms of the Zernike Polynomial Represented up to the 7th Order[19]

j = index	**n = order**	**m = frequency**	$Z_n^m(\rho,\theta)$	**Common Name**
0	0	0	1	Piston or Bias
1	1	-1	$2\rho \sin\theta$	Tilt y
2	1	1	$2\rho \cos\theta$	Tilt x
3	2	-2	$\sqrt{6}\,\rho^2 \sin 2\theta$	Astigmatism y
4	2	0	$\sqrt{3}\,(2\rho^2-1)$	Power
5	2	2	$\sqrt{6}\,\rho^2 \cos 2\theta$	Astigmatism x
6	3	-3	$\sqrt{8}\,\rho^3 \sin 3\theta$	Trefoil y
7	3	-1	$\sqrt{8}\,(3\rho^3-2\rho) \sin\theta$	Coma y
8	3	1	$\sqrt{8}\,(3\rho^3-2\rho) \cos\theta$	Coma x
9	3	3	$\sqrt{8}\,\rho^3 \cos 3\theta$	Trefoil x
10	4	-4	$\sqrt{10}\,\rho^4 \sin 4\theta$	Tetrafoil y
11	4	-2	$\sqrt{10}\,(4\rho^4-3\rho^2) \sin 2\theta$	Secondary Astig y
12	4	0	$\sqrt{5}\,(6\rho^4-6\rho^2+1)$	Primary Spherical
13	4	2	$\sqrt{10}\,(4\rho^4-3\rho^2) \cos 2\theta$	Secondary Astig x
14	4	4	$\sqrt{10}\,\rho^4 \cos 4\theta$	Tetrafoil x
15	5	-5	$\sqrt{12}\,\rho^5 \sin 5\theta$	Pentafoil y
16	5	-3	$\sqrt{12}\,(5\rho^5-4\rho^3) \sin 3\theta$	Secondary Trefoil y
17	5	-1	$\sqrt{12}\,(10\rho^5-12\rho^3+3\rho) \sin\theta$	Secondary Coma y
18	5	1	$\sqrt{12}\,(10\rho^5-12\rho^3+3\rho) \cos\theta$	Secondary Coma x

[19] "36 Terms of the Zernike Polynomial Represented u to the 7th Order." No Date. Online Table, modified. Standards for Reporting the Optical Aberrations of Eyes. 25 October 2005 <http://research.opt.indiana.edu/Library/VSIA/VSIA-2000_taskforce/TOPS4_2.html>

19	5	3	$\sqrt{12}\,(5\rho^5-4\rho^3)\cos 3\theta$	Secondary Trefoil x
20	5	5	$\sqrt{12}\,\rho^5\cos 5\theta$	Pentafoil x
21	6	-6	$\sqrt{14}\,\rho^6\sin 6\theta$	Pentafoil y
22	6	-4	$\sqrt{14}\,(6\rho^6-5\rho^4)\sin 4\theta$	Secondary Tetrafoil y
23	6	-2	$\sqrt{14}\,(15\rho^6-20\rho^4+6\rho^2)\sin 2\theta$	Tertiary Astig y
24	6	0	$\sqrt{7}\,(20\rho^6-30\rho^4+12\rho^2-1)$	Secondary Spherical
25	6	2	$\sqrt{14}\,(15\rho^6-20\rho^4+6\rho^2)\cos 2\theta$	Tertiary Astig x
26	6	4	$\sqrt{14}\,(6\rho^6-5\rho^4)\cos 4\theta$	Secondary Tetrafoil x
27	6	6	$\sqrt{14}\,\rho^6\cos 6\theta$	Pentafoil x
28	7	-7	$4\,\rho^7\sin 7\theta$	
29	7	-5	$4\,(7\rho^7-6\rho^5)\sin 5\theta$	
30	7	-3	$4\,(21\rho^7-30\rho^5+10\rho^3)\sin 3\theta$	Tertiary Trefoil y
31	7	-1	$4\,(35\rho^7-60\rho^5+30\rho^3-4\rho)\sin\theta$	
32	7	1	$4\,(35\rho^7-60\rho^5+30\rho^3-4\rho)\cos\theta$	
33	7	3	$4\,(21\rho^7-30\rho^5+10\rho^3)\cos 3\theta$	Tertiary Trefoil x
34	7	5	$4\,(7\rho^7-6\rho^5)\cos 5\theta$	
35	7	7	$4\,\rho^7\cos 7\theta$	

1. Strehl Ratio

The Strehl Ratio is the ratio of a laser's actual peak intensity to the intensity the laser would produce without any atmospheric aberration. When compensation for aberrations is perfect, the Strehl ratio would be one (unity).

In other words, the Strehl ratio details the ratio between the intensity at the point of maximum intensity in the observation plane, also known as the Gaussian point, and the intensity without aberration. This is indicated with the zero component of the Fourier transform ($e^{-2\pi j(f_x x+f_y y)}=1$). The Strehl ratio is given by the equation

$$S = \frac{1}{2\pi}\left|\int_0^{2\pi}\int_0^1 e^{(2\pi j\Delta W(\rho,\theta)\rho d\rho d\theta}\right|^2$$

The wavefront aberration relative to the reference sphere for diffraction focus is denoted by ΔW. Using the Taylor series, the Strehl ratio becomes

$$S = \frac{1}{2\pi}\left|\int_0^{2\pi}\int_0^1\left[1 + 2\pi j\Delta W + \frac{1}{2}(2\pi j\Delta W)^2 + \ldots\right]\rho d\rho d\theta\right|^2$$

$2\pi\Delta W$ can be eliminated from the equation if the aberrations are very small. This allows orders above second order to reduce to (where σ is in the unit of the wave)

$$S \simeq \left|1 + 2\pi j\overline{\Delta W} - \frac{1}{2\pi}(2\pi)^2\overline{\Delta W^2}\right|^2 \simeq 1 - (2\pi)^2\left[\overline{\Delta W^2} - \overline{(\Delta W)}^2\right] \simeq 1 - (2\pi\sigma)^2$$

For Strehl ratios less than .5, the approximation is no longer valid and the approximation shown by $S \simeq e^{\left[-(2\pi\sigma)^2\right]}$.

THIS PAGE INTENTIONALLY LEFT BLANK

VII. DEVELOPING THE TEST BED

A. DESIGN

The Adaptive Optics test bed went through several different iterations before a working design was implemented. Due to lack of space, the test bed was designed to fit in a small area, which made it harder to adjust the components. In order to have a working system several steps were taken.

1. Developing the Design

The design of the test bed was dependent on available space, funding and components on hand. The available space was small, 40"x25" on a semi-portable breadboard. The deformable mirror and the wavefront sensor were purchased through OKO technologies and were chosen to give the greatest ability for the cost of the equipment. Since both components were purchased from the same manufacturer, it was ensured that they would function together, and no additional parts or coding would be necessary to get them working as a unit. Other components available to the lab were several size mounts, translation bases and two achromatic lens kits ranging from a focal length of 20mm to 400mm.

The first step in developing the test bed was to create a rough draft of what the table needed to look like including developing the initial calculations for lens placements. The first draft was initially implemented on a vibration control table also being used for jitter control. The space was difficult to use because of its location and the test bed was moved to a simple optics breadboard of dimensions 40”x25”. A second design was developed for the new breadboard (shown below).

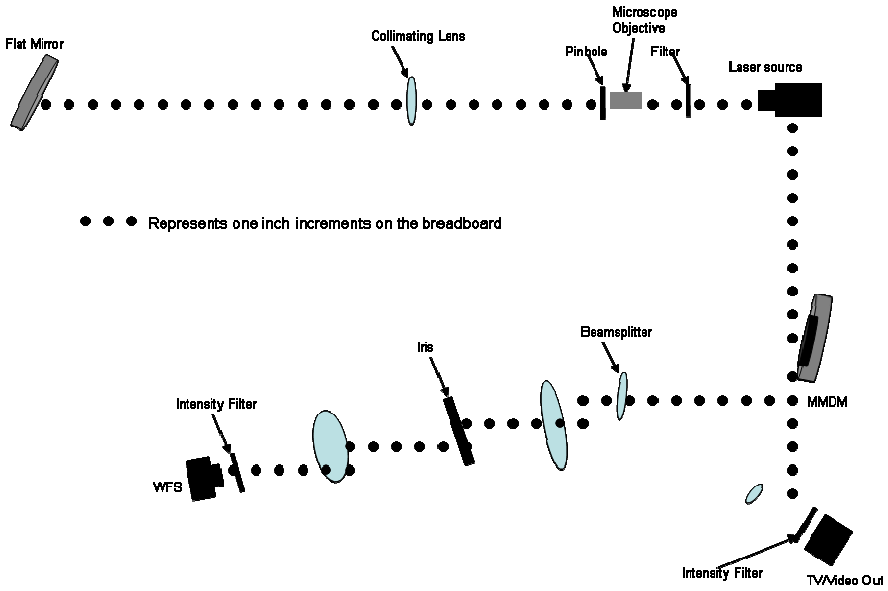

Figure 22. Table Layout

2. Collimating the Beam

The first thing to be done in order to implement the design was to collimate the beam. Collimation of a beam is a method designed to ensure a source with a planar wavefront by getting rid of the intensity variations and aberrations associated with the beam. To collimate the beam, the focal points of the microscope objective and the collimating meet need to be overlapped.

For the purposes of this test bed, the focal length of the microscope objective is 8mm and the focal length of the collimating lens was 250mm. The focal length of the microscope objective was determined by the equation $f = 160mm / Magnification$, where 160mm is the standard imaging configuration with an image location of 160mm from the back of the focal plane. For the different sized microscope objectives available, the following table gives the corresponding focal lengths.

Table 2. Microscope Objective Focal Lengths

Magnification (M)	Focal Length (*f*)
x5	32mm
x10	16mm
x20	8mm
x40	4mm
x60	2.7mm

Due to the fact that the breadboard is marked in English units, the focal lengths were converted to .3149 inches for the microscope objective and 9.8425 inches for the lens. For a perfectly collimated beam, the distance between the microscope objective and the collimating lens needed to be exactly 10.1575 inches, which dictated the need for translation bases.

In order to collimate the beam properly, several things need to be done. First, all of the optical components need to be at the same height.

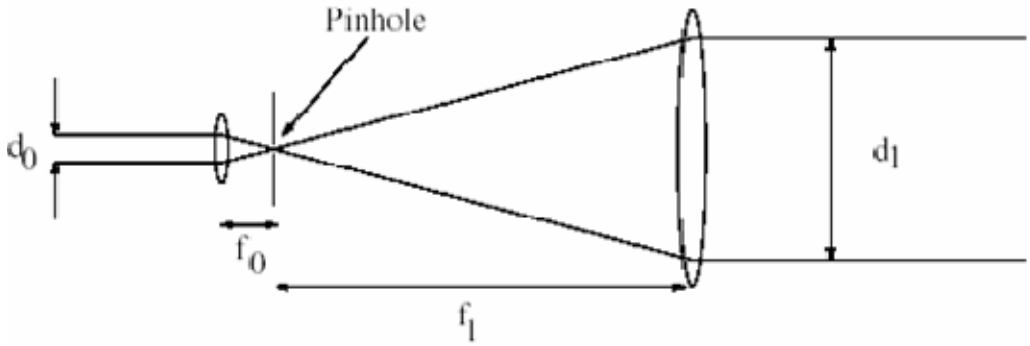

Figure 23. Collimation and expansion of the beam[20]

There are several ways to set the height of the beam; the two most common methods are with a ruler or with a set of irises.

[20] "Beam Expansion and Collimation". 24 August 1998. Online Image. Beam Expansion. 30 October 2005. <http://www.ph.ed.ac.uk/~wjh/teaching/optics-lab/Beam//beam-expand.pdf>

a. Setting the Height with Irises

To use the irises, first set the deformable mirror to the height you want to use it. Then set the irises to fall directly in the middle of the mirror (ensure the bases are attached to the irises). It may be easier to set all the components of the test bed to the approximate height of the irises before continuing. Set the first iris in front of the laser and adjust the laser to the height of the iris. The laser should have tip/tilt controls and be on a moveable base. Set the other iris far away from the first in the path you want the beam to travel (see picture). Close the irises to the smallest setting. By moving the base of the laser and the lateral movement control, adjust the beam so that it travels directly through both of the irises. Once the laser height is set, tighten it to the table and do not move it again.

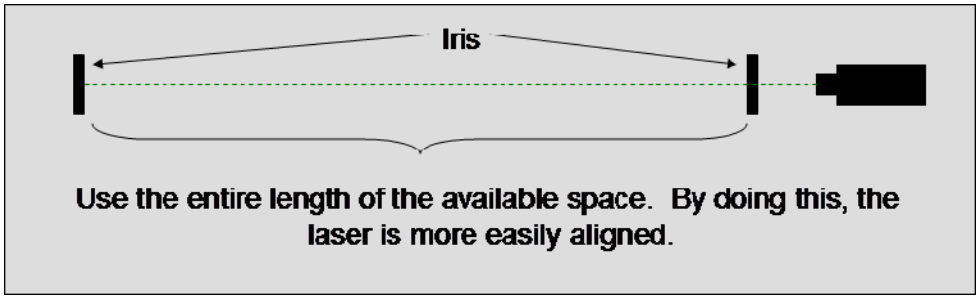

Figure 24. Aligning the laser using irises.

Next, insert the microscope objective. The microscope objective does not need to be a specific distance from the laser but needs to fall in the path of the beam. It also does not need to be on a translation stage but should be on an adjustable base. Adjust the height of the microscope objective so that the light once again falls through the center of both irises. To double-check the setting of the microscope objective, check the light that is being reflected back toward the first iris. When properly adjusted, this light should fall directly in the center of the iris. When the microscope objective is set, insert the pinhole.

The pinhole should be mounted using an xyz translation stage and an iris with tip/tilt control. The pinhole should be approximately 8 mm from the microscope objective. First, adjust the pinhole so that the light traveling through the iris and the microscope objective falls on the center of the pinhole. Next, using the tip/tilt controls,

ensure that the pinhole is planar (completely vertical). Using the translation controls, move the pinhole in the x direction until the light coming through the pinhole becomes very bright. This will take some time, and may require movement in the y and z directions as well. The light coming through the pinhole should be focused directly in the center of the second pinhole.

Finally, insert the lens into the path of the beam at the proper focal length and adjust the height to the same height of the beam. The focal length of the collimating lens was 250 mm, which is approximately 10 inches, which can be counted out on the breadboard fairly easily (The collimating lens should be a doublet.). The lens should be adjusted by hand until the center of the beam coming through the pinhole falls through the center of the second iris. Again, double-check by making sure the reflected light falls on the center of the pinhole.

A beam is collimated properly when the focal point of the light goes to infinity. In order to achieve this, use a mirror to focus the light on a far wall. Using a translating base, move the lens either back or forward until the focal point of the light goes to the point on the wall. The easiest way to locate the focal point is to use a piece of white paper. Drag the paper along the beam until the light comes to a point. Move the lens and repeat until the beam is no longer coming to a point before it reaches the wall.

b. Setting the Height with a Ruler

To set the height of the table with a ruler, carefully mark the height of the laser beam or light source on the ruler and compare it to the height of the beam exiting the microscope objective. The center of each component that is placed on the table should be at this height. The light then needs to be measured as it exits the collimating lens and matched to the exact height of the microscope objective. The purpose of this is to try to get a fully collimated beam of light coming from the lens.

The collimated beam can be checked several ways. The first is to use a simple white piece of paper to check if the beam was converging or diverging. This is very tedious, requires a significant distance from the aperture, and can yield poor results. The second, easier way is to take two pieces of computer perfboard and separate them by

some distance. The perfboard can be positioned in the collimated beam with a black piece of cardboard behind. This also requires some distance but is easier to use and doesn't need to be moved. As the rays of light show through the perfboard, they create circles on the black surface. The circles are actually rings with small dots in the center. When all of the circles looked the same, this shows that the beam is collimated. To eliminate the junk in the beam, a pinhole is used to create a spatial filter.

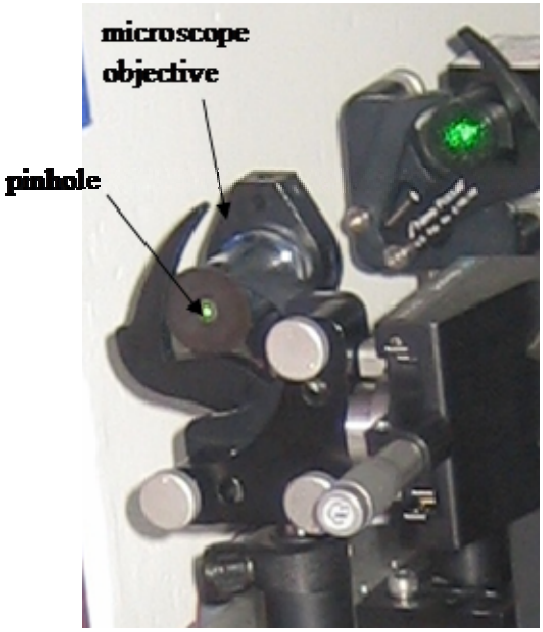

Figure 25. Pinhole and microscope objective

To position the pinhole correctly, first the pinhole needed to be as flat as possible. This was done by removing the microscope objective and using the tip-tilt adjusters to align the reflection off of the pinhole back to the center of the laser aperture. When this is done, place the microscope objective back in the system and the correct height and adjust it to point straight. Then use the translator to move very slowly in the x direction until the pinhole is at the focal length. The position of the focal length can sometimes be determined by the light impinging on the pinhole. As the pinhole reaches the correct placement, this light will reach maximum intensity. To double-check this, the beam of light coming out of the pinhole should be checked for divergence. The beam must diverge toward the lens.

Regardless of which method being used proper collimation of the beam can be checked with a shear plate. Position the shear plate in the path of the beam after the lens so that the translucent plated can be seen. The collimated light should create straight black lines called fringes across the circle of light in the plate. Turn the plate on its side and check it again. Adjust the lens in small amounts using the x translation stage. When straight fringes can be seen in both positions, the beam is collimated.

3. Adding the Wavefront Sensor

After the beam is properly collimated, the next step is to insert the wavefront sensor into the system. The wavefront sensor being used is a Shack-Hartmann wavefront sensor manufactured by Basler and distributed by OKO Industries (see chapter IV). The software program Front Surfer came with the sensor to be used for analysis.

A series of two inch diameter flat mirrors were used to route the beam to the sensor. Before inserting the MMDM, the wavefront sensor was attached and calibrated. The initial calibration shows how the reference grid used by the sensor to determine the slope of the wavefront as it impinges on the lenslet array. The graph shown below shows the phase of the wave. On the first test bed, a red diode laser of 670nm wavelength was used. This was later changed to a green laser of 532nm. The initial calibrations were done using the 670nm red diode laser. The red laser was not powerful enough to sustain a beam very far and the beam was not very good quality. Another calibration with the green laser was done later.

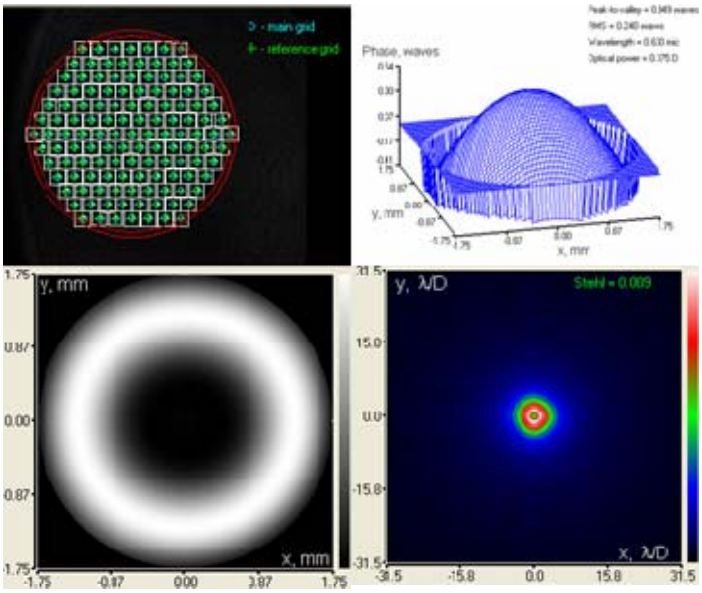

Figure 26. Initial calibration run with red laser

After calibrating the wavefront sensor, the system is ready for the deformable mirror. Although the design eventually calls for two mirrors, only one will be used for the calibrations of the system.

4. Connecting the Deformable Mirror

After the beam was collimated and the wavefront sensor calibrated, the test bed was ready for the deformable mirror. The mirror being used is a Micro-Machined Deformable Mirror developed by OKO Technologies (see chapter IV).

a. Building the Power Supply

To operate the mirror, a power supply had to be built. The shape of the mirror is controlled by two identical high voltage power amplifier boards, which were purchased with the mirror. The two boards contained 20 non-inverting DC amplifiers each. The schematic, also purchased with the mirror, show how the unit needed to be configured and are in Figure 27.

As per the schematics, the amplifier boards were connected to a high power voltage supply and a +/- 15 V power brick purchased from a local electronics store.

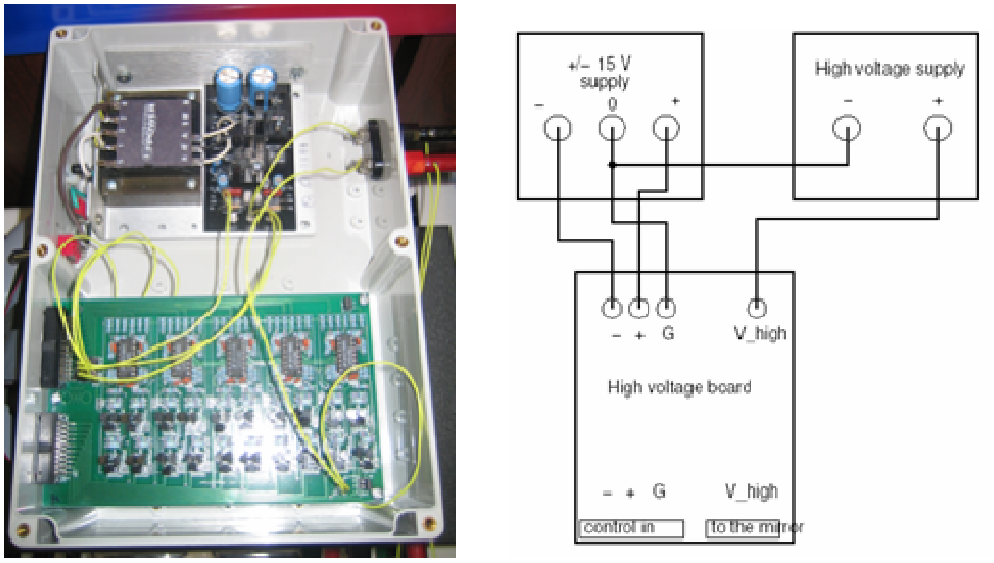

Figure 27. Mirror power supply and schematic[21]

The two PCI boards were inserted into the computer and in accordance with the instructions the PCI boards were connected to the power supply. It was in turn connected to the mirror.

The fully constructed test bed is shown below.

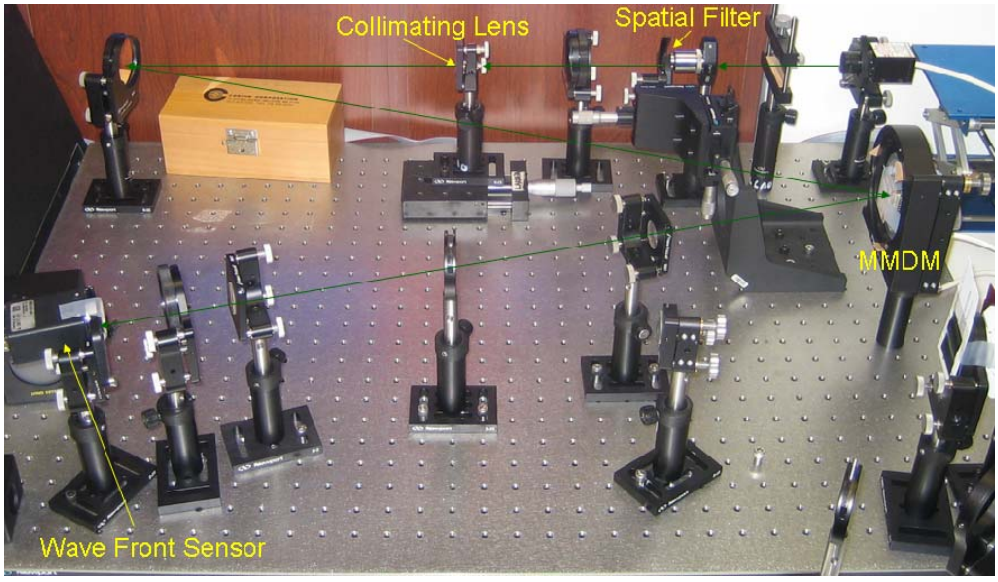

Figure 28. Adaptive Optics Test bed

[21] Technical passport.

THIS PAGE INTENTIONALLY LEFT BLANK

VIII. OPERATION OF THE TEST BED

A. USING FRONTSURFER

The wavefront sensor and mirror were controlled with a program called FrontSurfer. FrontSurfer was developed by OKO Industries specifically to be used with their components.

1. Wavefront Reconstruction

Wavefront reconstruction is the process of restoring a distorted wavefront to its planar form. Using FrontSurfer, the distorted wavefront is represented graphically as a potato-chip like structure. The source light in this instance is to be considered a point source being aberrated or distorted by turbulence in the atmosphere as the light passes through. The wavefront sensor measures the shape of this incoming wavefront and the deformable mirror reconstructs the wavefront by "matching" the shape of the mirror to the shape of the wavefront. Adaptive optics is solves the problem of what data is needed in order to force the deformable mirror to shape itself correctly to cancel out the disturbance in the wavefront. This is usually done by discretely sampling the wavefront with a wavefront sensor. The sensor being used is capable of reconstructing wavefront profiles with an RMS sensitivity of $\lambda/40$ before calibration and $\lambda/80$ after minimal calibration.

The lenslet array inside the sensor forms a matrix and records where the light falls on the quad cells (pixels). The camera samples the changes in the distribution of the light and the slopes of the change in this light are found by adding the differences in the light falling on each pixel in the quadcells. The subapertures of the OKO wavefront sensor are centered with less than $1\mu m$ error and are imaged using a high-resolution Basler CCD camera. The result is a series of orthogonal slopes that are particular to each quadcell. To efficiently perform the functions required to obtain these slopes, it is most effective to place the mirror in a position where it is at a point conjugate to where the atmospheric disturbance is being sampled.

The array from each quadcell is expressed in equation form as $M^{x_{11}} = (N_{12} + N_{22} + N_{11} + N_{21})$ in the x direction and $M^{y_{11}} = (N_{11} + N_{12} + N_{21} + N_{22})$ in the y direction. N is the position of the node and M is the slope measured in the x and y direction of each quadcell. The sensor being used applies an algorithm that uses a finite-difference approach, which means the function from reconstruction of the wavefront will not be continuous.

Using M vector equations, a matrix formulation is be constructed, $M = A * N$. M *and* N are represented in the form of column vectors, and A represents the relationship between the quadcell and the node, with columns and rows of *m x n* where $m \neq n$.

As the wavefront sensor detects the incoming data, the matrix A is inverted to obtain the nodes ($N = A^{-1}M$). It does this by performing a least squares approximation of the matrix, which minimizes the error across the wavefront. The OKO wavefront sensor being used has 37 actuators and a mask size of 10mm x 10mm, and 128 quadcells which will generate a relatively small matrix for an AO system of $37 * (256) = 9472$ elements. A problem can occur during least squares approximation when the matrix is not singular or square. This problem is sorted out by using the transpose of the A matrix where $A^T xA$ is used to incorporate Singular Value Decomposition. The nodal equation then becomes $N = [(A^T A)^{-1} A^T]M$, known as the control matrix for the AO system. The wavefront sensor uses the matrix N to estimate the phase change at each node of the wavefront.

2. Calibrating the Sensor and Mirror

Before using the test bed, both the wavefront sensor and the mirror need to be calibrated. Both of these functions can be accomplished through FrontSurfer.

a. Calibration the sensor using two points of recognition

FrontSurfer uses two preset hexagonal sources to calibrate the wavefront sensor. To use this feature, go to "Options" $\rightarrow$ "Parameters", set the source to "file", and the reference grid to 'hexagonal". Change the number of spots to 19 by setting the reference

grid order to 3, and enter a wavelength (for simplicity, make the wavelength equal to the wavelength of the laser being used, in this case 532nm). At the bottom of the screen, push "Calibrate"; set the distances to .5m and 1m respectively and load the two packaged calibration files (for this sensor, the files are cal50.bmp and cal100.bmp). After the two grid patterns appear on the screen, push "start". When the program finishes running, push "ok". Return to "Options"→"Parameters" and set "Radius of the Reconstruction area" to .95, change "Number of Zernike terms" to 14, and "Smoothing filter size" to 10. Ensuring "Ignore Defocus" is not pressed, go to "File"→"Open Main" and reload cal50.bmp. Push the blue arrow on the button bar to show the reconstructed wavefront. The sensor has now been calibrated. (Vdovin, 20-21)

b. Calibrating the Mirror

The mirror should be calibrated before each run to ensure all the actuators are correctly aligned. To do this, first go to "Mirror"→"Set Values" and make sure all values are set to zero. Next go to "Mirror"→"Target Function" and make sure that there are no functions set. To do this, click on whatever is in the box and click "delete". Next go to "Mirror"→"Calibrate". This will calibrate the mirror and will also allow the feedback mode to be used.

3. Deciphering the Data

a. Phase Graph

This graph represents the change in phase of each portion of the wavefront as they impinge on the lenslet array inside the senor. It provides data concerning the error of the wavefront caused by aberrations in the beam.

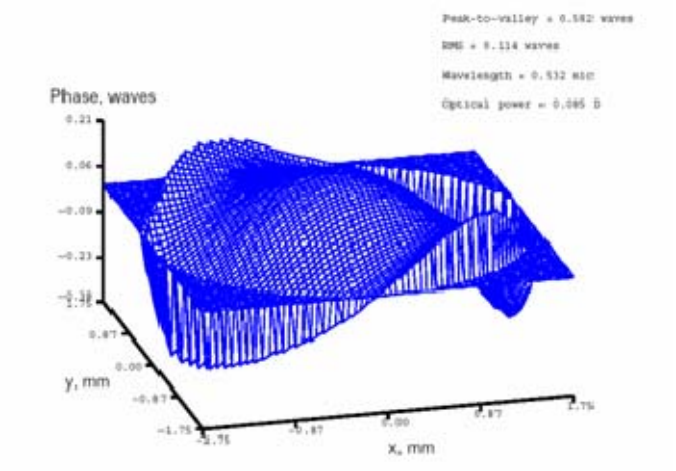

Figure 29. Isometric Surface Plot Wavefront Phase Change

(1) Peak-to-Valley Error. Peak-to-valley wavefront aberration description is useful when working with aberrations higher than third-order or when more than one aberration is present. Peak-to-valley indicates the maximum distance of the desired wavefront from the actual wavefront both in the negative and the positive direction. In other words, it is the difference between the highest and lowest parts of the wavefront. If the maximum difference in the negative direction is -.25 waves and the maximum difference in the positive direction is +.1 waves then the peak-to-valley error is .35 waves. The standard for peak-to-valley error set by Sir Raleigh in the late 1800's was considered to be $(1/4)\lambda$. It was said that when PV error was $(1/4)\lambda$ it was diffraction limited. This means that if the PV error exceeds ¼ of the wavelength, the optical quality will start to degrade. Recent technological discoveries have made it possible to adjust the diffraction limited quality of an aperture to as high as PV $(1/10)\lambda$ *to* $(1/10)\lambda$. Even with advances in technology, this method of determining wavefront error can be problematic because it does not specify the area over which the error is occurring. A system can have a large peak-to-valley error and perform better than a system with a small peak-to-valley error. This is why using the RMS wavefront error can sometimes be more helpful.

(2) RMS Error. RMS or root mean squared error tells you how much the height varied over the entire wavefront. Taking the RMS of a wavefront means taking the square of the wavefront error, averaging it over the entire wavefront,

then taking the square of that. For a circular pupil, the RMS wavefront error expressed in Zernike terms is given by the equation

$$rms = \frac{1}{\pi}\int_0^{2\pi}\int_0^1 \left[\Delta W(\rho,\theta) - \overline{\Delta W}\right]^2 \rho d\rho d\theta = \overline{\Delta W^2} - \left(\overline{\Delta W}\right)^2$$

where ρ and θ are the polar coordinates of the unit circle representing displacements in the image plane or the exit pupil and W represents the wavefront being degraded. Maréchal determined an optical "system to be well corrected if when the normalized intensity at the diffraction focus is greater or equal to .8." (Born and Wolf, 528) Marechal was a French physicist who in 1947 described the error of a wavefront by measuring the ratio of the error size to the overall aperture size. Using this criterion, the focus can be given by $(F) \geq .8 \; when \; \Phi_F \sim\leq \lambda/14$ where Φ_F denotes the aberration function. Based on this, the system is said to be diffraction limited when the rms error does not exceed $\lambda/14$.

b. Far-Field Intensity

The diffraction pattern seen in the far-field graph somewhat resembles a bull's-eye where the center ring is the Airy disc which is surrounded by several less distinct rings, each separated by a region of zero intensity.

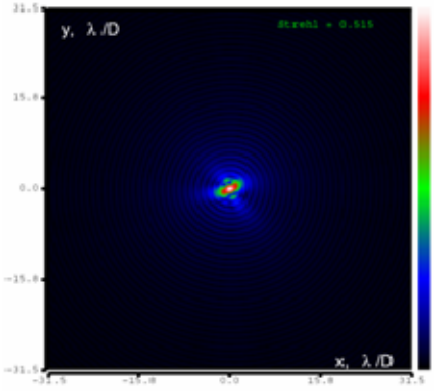

Figure 30. Far-Field Intensity Graph

This diffraction pattern describes the limitation of the circular lens. The limiting spot size of the aperture is determined by the f/# of the lens given by the equation $d = 2.44\lambda(f/\#)$. The peak irradiance in the beam, combined with the J1 Bessel function (of the first order), is used to describe the irradiance distribution as given in the equation $I_x = I_o\left[\frac{2J_1(x)}{x}\right]^2$. The Bessel function is described by the equation $J_1(x) = x\sum_{n=1}^{\infty}(-1)^{n+1}\frac{x^{2n-2}}{(n-1)!n!2^{2n-1}}$ where $x = \frac{\pi D}{\lambda}\sin\theta$ (θ is the angular radius from the diffraction maximum, and D represents the diameter of the circular aperture). The smallest spot size that can be achieved for an aperture with a specific f-number can be determined by finding the angular radius $\sin\theta = \frac{x\lambda}{\pi D}$. The value of x for each ring is related to the intensity and energy by the following table. This table depicts the distribution for a perfectly circular aperture. Many times, the far-field does not appear perfectly circular due to imperfections in the aperture or improper alignment of the beam.

Table 3. Energy distribution for a perfectly circular aperture[22]

Ring	Position (x)	Percentage of Energy in the ring	Relative Intensity (I/I_o)	Max/Min
Airy Disc	0	83.8	1	Max
First Dark	3.833		0	Min
First Bright	5.136	7.2	.0175	Max
Second Dark	7.016		0	Min
Second Bright	8.417	2.8	.0042	Max
Third Dark	10.174		0	Min
Third Bright	11.620	1.5	.0016	Max
Fourth Dark	13.320		0	Min
Fourth Bright	14.797	1.0	.0008	Max
Fifth Dark	16.462		0	Min

The Strehl ratio (See Chapter VI) is given in the upper right-hand corner of the graph. The size of the Airy disk is directly related to the Strehl ratio. The Airy disk can be found using the relation $D = 2.44\lambda(f/\#)$. Apertures where the defects are

[22]; Melles Griot, Inc. "Energy Distribution in the Diffraction Pattern of a Circular or Slit Aerture." No Date. Online Table. 30 October 2005. <http://www.mellesgriot.com/pdf/001.20-1.22.pdf> (Modified with information from Born and Wolf, 441)

minimal to the point where they cause less blur than the Airy Disk are diffraction limited. When this occurs, the Strehl ratio will be 1. As previously stated, the Strehl ratio is the ratio between the peak Gaussian intensity of an image divided by the peak intensity of a diffraction-limited image, or the ratio of peak focal intensities in the aberrated and ideal point spread functions (Born and Wolf, 520). The Strehl ratio can be stated in terms of the RMS error where $S \equiv e^{-(2\pi\sigma)^2}$. This is because, for small aberrations, the Strehl ratio is related to the change in phase aberration by $S \simeq 1 - \sigma_\phi^2$. The closer the Strehl ratio is to 1, the less the error due to aberration.

c. Interferometery Data

Wavefront data from the Shack-Hartmann sensor is relayed to the computer in matrix form which consists of an array of numbers; sometimes hundreds of numbers. To help visualize this data, FrontSurfer converts the data to a topographical wave representation in two dimensions similar to the one shown below. This graph shows the wavefront slopes as measured in the x and y directions, which corresponds to the wavefront error values across the pupil.

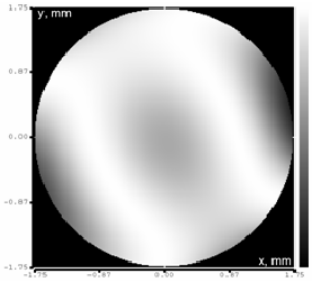

Figure 31. Interferometric Representation of Wavefront Error

4. Troubleshooting FrontSurfer

Common problems encountered with FrontSurfer are alignment, inability to perform iterations due to saturation, and the error message "maximum spot displacement exceeds average distance between spots."

There is an easy way to tackle alignment using FrontSurfer. There is a loop feature on FrontSurfer that will show several lower order aberrations in graph formation and allow fine tuning of the system.

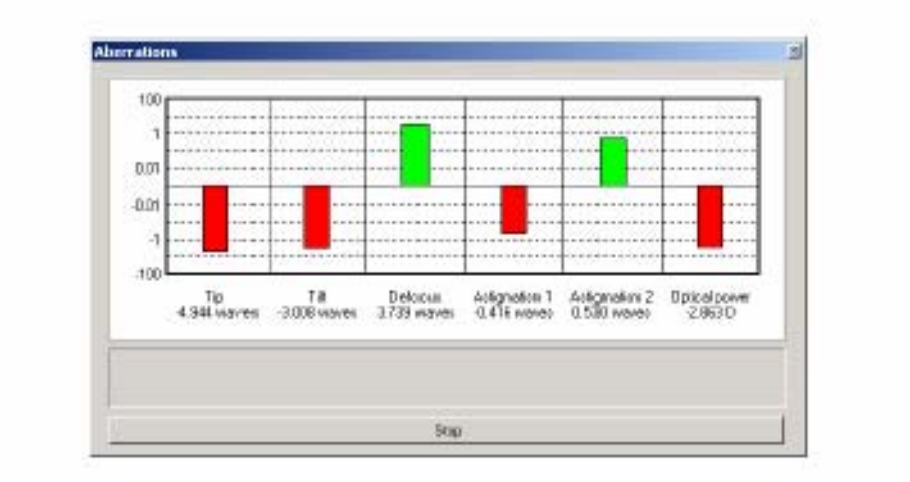

Figure 32. Loop Feature on Frontsurfer

To use this feature, open FrontSurfer, open "Processing" → "Loop", click in each box except power and click ok. Turn the monitor so it can be seen from the test bed and while watching the graphs, carefully move the collimating lens back or forward to eliminate defocus. Then use the y and z translation on the collimating lens to help eliminate as much of the coma, astigmatism, and spherical aberration in the system as possible.

The easy solution to eliminate saturation is to use neutral density filters. The best position to use the filters is directly in front of the wavefront sensor. Eliminating the saturation will increase the accuracy of the wavefront sensor. It will also help eliminate the error message "maximum spot displacement exceeds average distance between spots."

B. EXPERIMENTAL RESULTS

To induce aberrations into the beam, a beam splitter was used because of the spherical lens characteristics, which meant that the overriding aberration would most

likely be on the order of a spherical aberration. It would also induce other aberrations such as astigmatism and coma. The beam splitter was inserted between the spatial filter and collimating lens to simulate stimulation from an outside source. The aberration created using the beam splitter was then corrected using the deformable mirror. Before the induced aberration, the system was fine tuned using the loop feature until the wavefront was under .25 waves peak-to-valley, and the Strehl ratio was greater than .850. The aberration was induced into the system and then corrected back to under .25 waves peak-to-valley.

The results from the initial run after alignment are shown below. The picture on the left shows the reference grid used by the wavefront sensor to reconstruct the wavefront. The graph on the right shows the 3-d representation of the phase of the wavefronts.

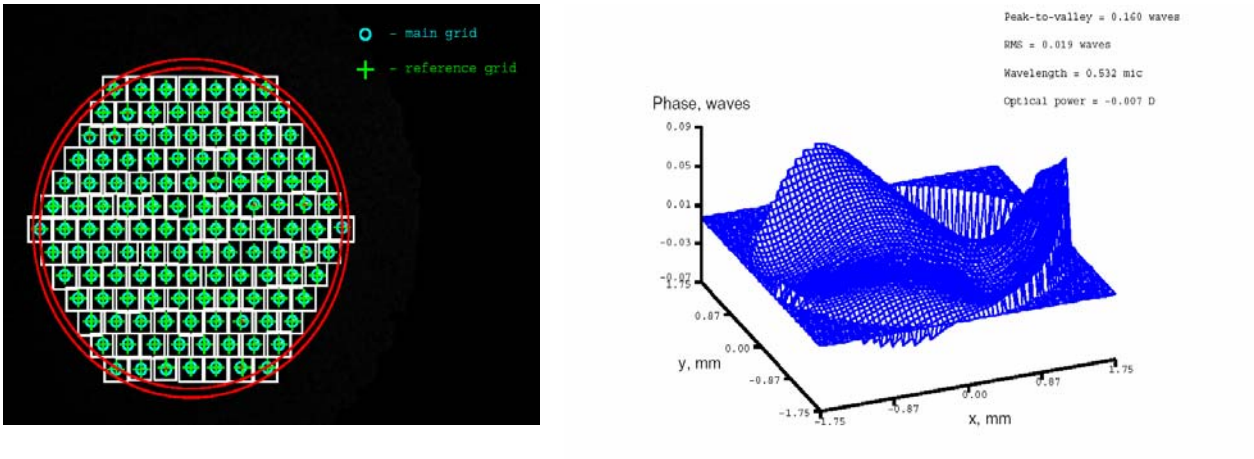

Figure 33. Baseline wave data

A perfectly planar wave would be shown as a flat graph with no 3-d features. The 'potato chip' image seen is a close to a planar wave that the system can achieve. As shown in the above graph, the peak to valley value was .160 waves and the rms error was .019 waves. The following graphs show the baseline far field and topographical data gathered.

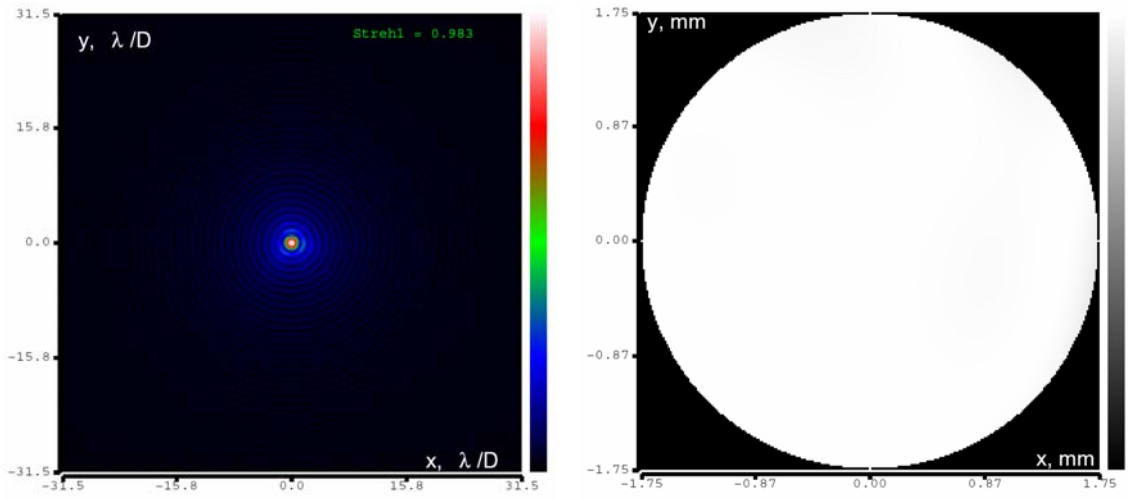

Figure 34. Baseline far field and interferometry data

The far field data shows a Strehl ratio of .983, which is very close to unity and the 2-d topographical graph shows almost no error across the wavefront. This does not mean there is no error, but that the error is relatively small and almost negligible. The data generated from the baseline graphs is as shown below. The table shows each of the lower order aberrations and their influence on the above shown graphs.

As seen in Table 2, the strongest error being detected by the system is C[4,-2], which is a secondary astigmatism in the y direction denoted by the equation $\sqrt{10}\rho^4(4\rho^4-3\rho^2)\sin(2\theta)$. Secondary astigmatism, being a fourth order polynomial is more difficult to correct for and some error is expected.

Table 4. Baseline Test Report

Test report, generated on
Thu Nov 17 04:01:21 PM

Parameters:

Decomposition area diameter = 3.675000e+000 mm
Reconstruction area diameter = 3.491250e+000 mm
Wavelength = 5.320000e-001 mic
Strehl factor: 9.829378e-001
Phase peak-to-valley = 1.601175e-001 waves
Phase RMS = 1.850185e-002 waves
Distance to focus = 1.410924e+002 m

Zernike coefficients:

C[1,1] = 0.000000e+000 waves (tip)
C[1,-1] = 0.000000e+000 waves (tilt)
C[2,0] = 1.124552e-002 waves (focus)
C[2,2] = -2.151153e-002 waves (astigmatism)
C[2,-2] = -3.834163e-003 waves (astigmatism)
C[3,1] = -7.359405e-003 waves (coma)
C[3,-1] = 2.462653e-002 waves (coma)
C[3,3] = -2.900275e-002 waves (trifoil)
C[3,-3] = 2.278954e-002 waves (trifoil)
C[4,0] = 8.264234e-003 waves (spherical aberration)
C[4,2] = -2.491674e-002 waves
***C[4,-2] = 3.280396e-002 waves
C[4,4] = 1.261737e-002 waves
C[4,-4] = 2.505822e-002 waves

Decomposition is made over the decomposition area (outer red circle).

Seidel aberrations:

Tilt = 0.000000e+000 waves {C*[1,1]^2 + C*[1,-1]^2}^1/2
Focus = 1.580836e-002 waves 2C*[2,0]
Astigmatism = 3.527653e-002 waves 2{C*[2,2]^2 + C*[2,-2]^2}^1/2
Coma = 6.583170e-002 waves 3{C*[3,1]^2 + C*[3,-1]^2}^1/2
Spherical aberration = 3.975741e-002 waves 6C*[4,0]

Seidel coefficients are calculated by integration over the reconstruction area (inner red circle).

Without recalibrating the mirror, the beam splitter was inserted into the system, and the wavefront reconstruction data was displayed once again in graphical form shown below.

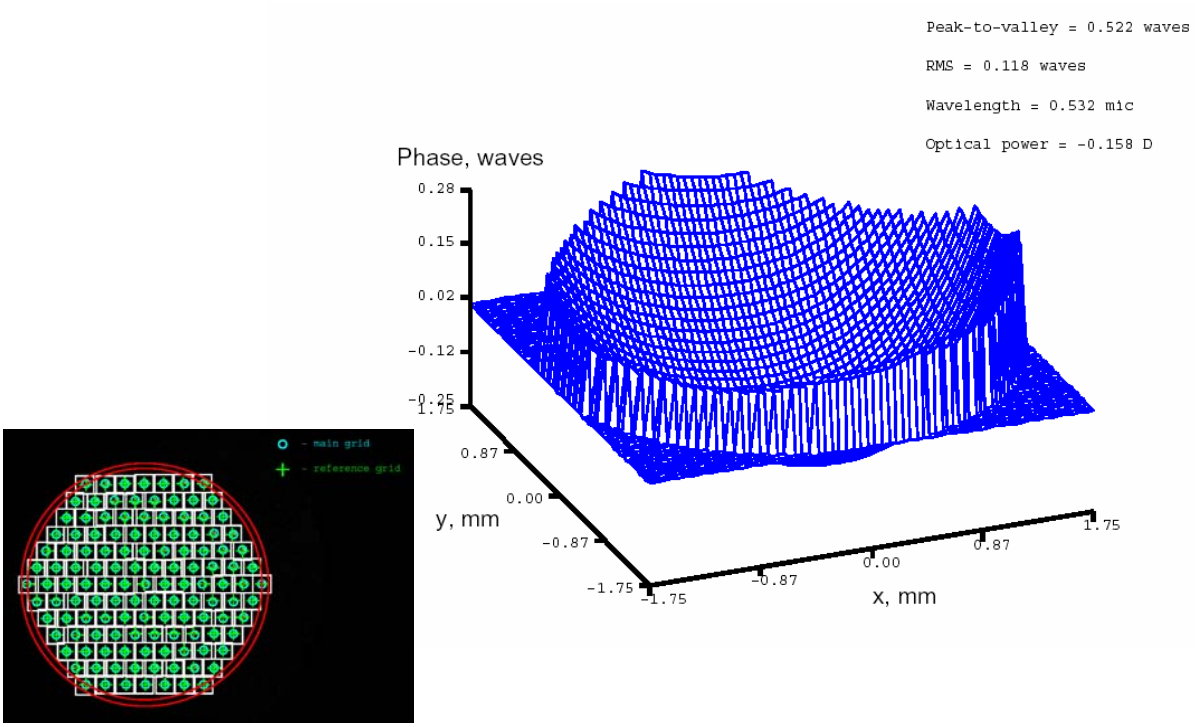

Figure 35. Wavefront data with aberration

The new peak-to-valley waves was .522 waves and the rms error was .118 waves which is almost 4 times more error than the baseline. The change of shape in the graph depicts a large deviation off of the base axis showing a significant change in phase error in the wavefront.

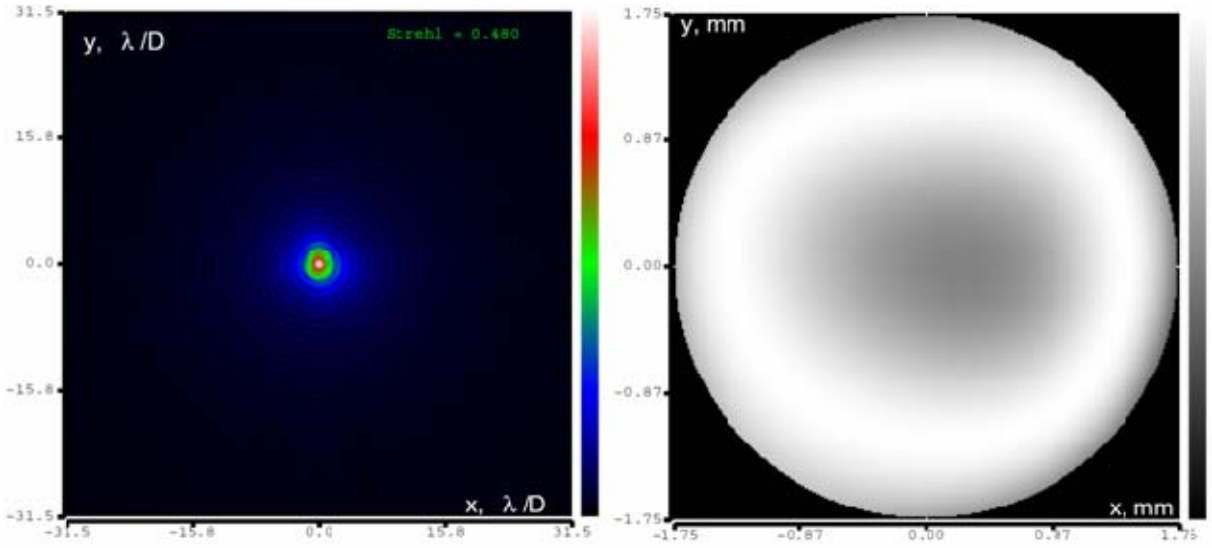

Figure 36. Far Field intensity and interferometry data with aberration

The new Strehl ratio was .480 which clearly shows a disturbance in the wavefront pattern. The difference between the aberrated wavefront and the baseline is clearly visible through the midsection of the interferometry pattern. The far field diffraction pattern shows the change in the Fraunhofer diffraction. The Airy disk is more spread out and somewhat elongated clearly showing that some sort of aberration is inherent in the system.

The report shows the difference in each type of lower order aberration detected by the system.

Table 5. Aberration Report

Test report, generated onThu Nov 17 04:04:09 PM

Parameters:

Decomposition area diameter = 3.675000e+000 mm
Reconstruction area diameter = 3.491250e+000 mm
Wavelength = 5.320000e-001 mic
Strehl factor: 4.800791e-001
Phase peak-to-valley = 5.222960e-001 waves
Phase RMS = 1.183480e-001 waves
Distance to focus = 6.328279e+000 m

Zernike coefficients:

C[1,1] = 0.000000e+000 waves (tip)
C[1,-1] = 0.000000e+000 waves (tilt)
***C[2,0] = 2.507249e-001 waves (focus)
C[2,2] = -2.034553e-002 waves (astigmatism)
C[2,-2] = -2.860821e-002 waves (astigmatism)
C[3,1] = 5.438254e-003 waves (coma)
C[3,-1] = 4.468494e-002 waves (coma)
C[3,3] = -2.491799e-002 waves (trifoil)
C[3,-3] = 1.403900e-002 waves (trifoil)
C[4,0] = 1.128606e-002 waves (spherical aberration)
C[4,2] = -2.443260e-002 waves
C[4,-2] = 4.312608e-002 waves
C[4,4] = 9.440613e-003 waves
C[4,-4] = 2.583447e-002 waves

Decomposition is made over the decomposition area (outer red circle).

Seidel aberrations:

Tilt = 0.000000e+000 waves {C*[1,1]^2 + C*[1,-1]^2}^1/2
Focus = 4.451465e-001 waves 2C*[2,0]
Astigmatism = 7.806164e-002 waves 2{C*[2,2]^2 + C*[2,-2]^2}^1/2
Coma = 1.153166e-001 waves 3{C*[3,1]^2 + C*[3,-1]^2}^1/2
Spherical aberration = 4.790273e-002 waves 6C*[4,0]

Seidel coefficients are calculated by integration
over the reconstruction area (inner red circle).

As indicated by the report, the main aberration influences from the beam splitter were defocus, spherical and coma in the x direction. The largest change was in the focus, a second order aberration given by $\sqrt{3}(2\rho^3-)$. Change in focus is expected due to

the fact that the beamsplitter is a lens, and is not cause for concern. The next largest changes occurred in coma in the y-direction given by $\sqrt{8}(3\rho^3 - 2\rho)\sin\theta$, spherical aberration given by $\sqrt{5}(6\rho^4 - 6\rho^2 + 1)$, and secondary astigmatism in the y-direction given by $\sqrt{10}(4\rho^4 - 3\rho^2)\sin 2\theta$. These 3 aberrations caused a significant change in the reconstruction of the wavefront.

Due to the fact that the beam splitter is a type of lens, defocus was expected and was easily corrected by the system. The spherical, astigmatism, and coma aberrations were more interesting and harder to correct. Because all of these are fourth order or below, FrontSurfer was able to correct for them as shown below.

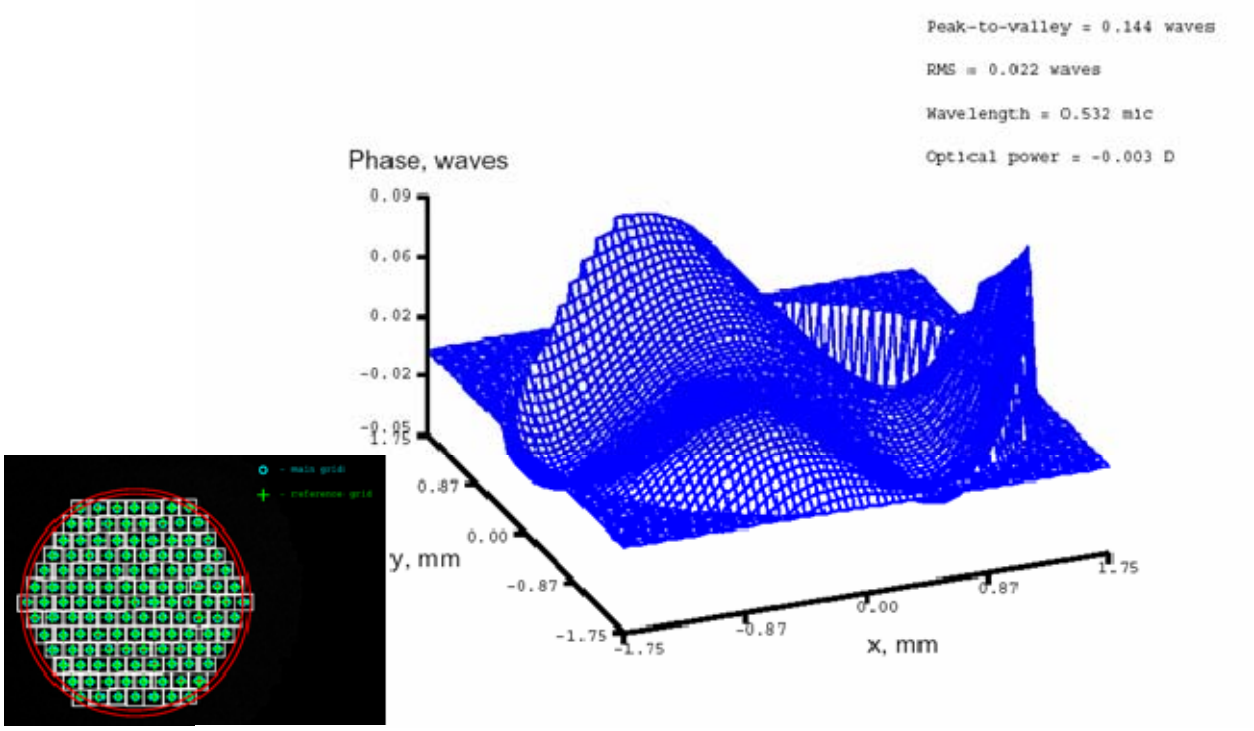

Figure 37. Wavefront data after correction

Using the deformable mirror and feedback from FrontSurfer, the system was able to correct the wavefront close to what it was originally. The peak-to-valley phase value returned to under a quarter wave becoming .144, slightly better than the original value of .160. More importantly, the rms error was now .022, very close to the original .019. The

difference in these values is negligible. Each time the system runs the values will be slightly different due to changes in the light in the room, the change in temperature in the room and other factors that are difficult to control in this setting. The focus in this experiment is on the large differences in the values and the drastic changes due to aberrations in the beam splitter. The RMS error is more indicative of what the system is doing because peak-to-valley only looks at the change in phase from wave to wave and does not take into account the area over which the error is occurring. The RMS error over the unit circle of the area being observed, indicated by the red circles on the graph is given by the equation

$$\sigma^2_{rms} = \left[\frac{1}{\pi}\int_0^{2\pi}\int_0^1 \Delta W^2(\rho,\theta)\rho d\rho d\theta\right] - \frac{1}{\pi}\left[\int_0^{2\pi}\int_0^1 \Delta W(\rho,\theta)\rho d\rho d\theta\right]^2$$

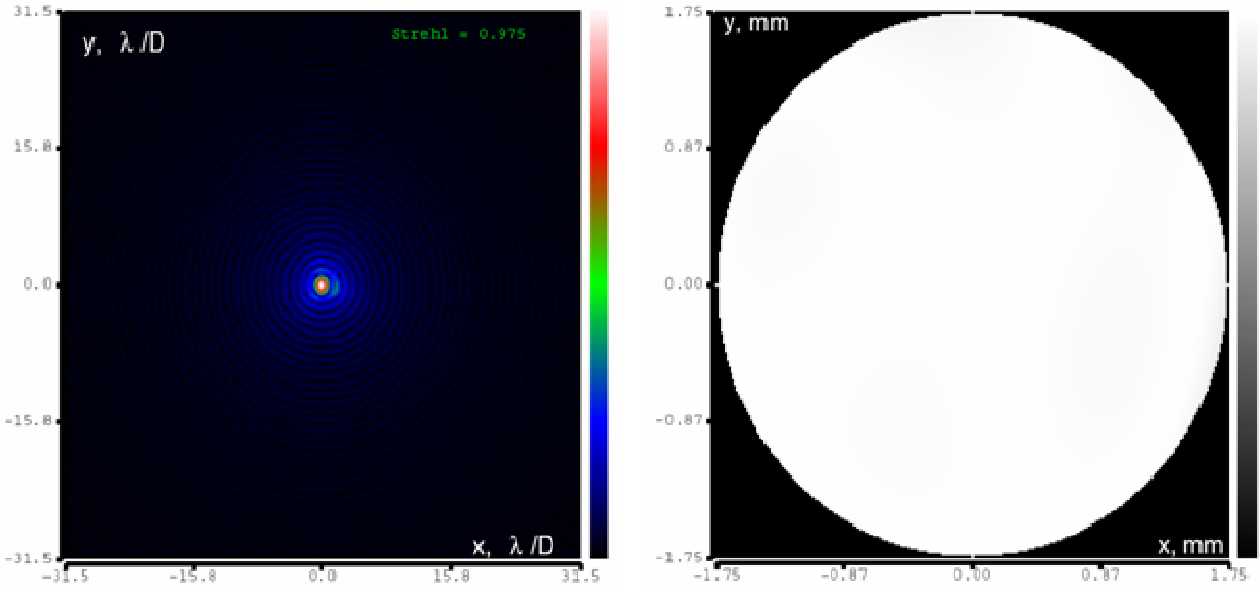

Figure 38. Far-Field Intensity and Interferometry Data

As shown on the above graphs, the corrected Strehl ratio was .975, very close to the baseline data of .983. The far-field or Fraunhofer diffraction pattern once again showed a small airy disk surrounded by very distinct fringes in a symmetric pattern. The corrected report is shown in the table below.

Table 6. Correction Report

Test report, generated on Thu Nov 17 04:06:10 PM

Parameters:

Decomposition area diameter = 3.675000e+000 mm
Reconstruction area diameter = 3.491250e+000 mm
Wavelength = 5.320000e-001 mic
Strehl factor: 9.752287e-001
Phase peak-to-valley = 1.437003e-001 waves
Phase RMS = 2.227744e-002 waves
Distance to focus = 3.099524e+002 m

Zernike coefficients:

C[1,1] = 0.000000e+000 waves (tip)
C[1,-1] = 0.000000e+000 waves (tilt)
C[2,0] = 5.119035e-003 waves (focus)
C[2,2] = -3.525961e-003 waves (astigmatism)
C[2,-2] = -1.883348e-002 waves (astigmatism)
C[3,1] = 2.261862e-003 waves (coma)
C[3,-1] = 3.228207e-002 waves (coma)
C[3,3] = -3.089151e-002 waves (trifoil)
C[3,-3] = 2.554300e-002 waves (trifoil)
C[4,0] = 1.499364e-002 waves (spherical aberration)
C[4,2] = -3.472561e-002 waves
***C[4,-2] = 3.740340e-002 waves
C[4,4] = 1.591729e-003 waves
C[4,-4] = 2.851771e-002 waves

Seidel aberrations:

Tilt = 0.000000e+000 waves {C*[1,1]^2 + C*[1,-1]^2}^1/2
Focus = 1.203945e-003 waves 2C*[2,0]
Astigmatism = 5.511260e-002 waves 2{C*[2,2]^2 + C*[2,-2]^2}^1/2
Coma = 8.285205e-002 waves 3{C*[3,1]^2 + C*[3,-1]^2}^1/2
Spherical aberration = 7.267827e-002 waves 6C*[4,0]

Seidel coefficients are calculated by integration over the reconstruction area (inner red circle).

As expected, the largest correction (.24560 waves) was focus. All of the aberrations were corrected to close to their original values, and once again Secondary astigmatism in the y direction was the largest error. These results were very satisfactory in that this test bed is prone to outside influence and error.

Several basic laboratory changes that can be made to lower influences from outside sources are screening out excess light and vibrationally isolating the test bed from the floor.

IX. CONCLUSIONS

Adaptive Optics is a very challenging field of study. The development of a system that can correct for any number of aberrations that are caused by turbulent atmosphere is very difficult to do. The test bed that was built for this thesis was a success in that it was able to take several different aberrations and correct them to within 98% of the baseline data.

This system, however, only considered the very basic form of aberrations that could be present, focusing on lower order Zernike forms (fourth order and below). The system is limited by the size of the matrix that can be formed by the reconstruction process and the size of the components being used. The deformable mirror limits the system by the number of apertures. Most high quality micromachined deformable mirrors have more than 100 actuators, whereas the mirror being used for this research has 37 actuators and is only 15mm in diameter. The number of actuators limits the size of the matrix that the wavefront sensor can produce. The wavefront sensor has an input diameter of 5mm, which means that a series of lenses needs to be used to reduce the size of the beam that is seen by the sensor.

Although this experiment in its rudimentary form was a success, many things can be done to improve the quality of the results. First, a higher quality sensor and mirror combination could greatly improve the overall function of the test bed. A program with a higher capacity for matrix formulation needs to be used to be able to construct higher-order matrices and Zernike polynomials. Ideally, this program would be more user-friendly, as FrontSurfer is not always easily understood and there is not a great deal of information concerning the intricacies of the program.

Other more minor changes to the test bed would be helpful as well. This includes a better power supply for the laser. The laser being used in the test bed is a high-quality green laser, however, the power supply causes it to pulse. The reflection back from the microscope objectives and lenses also caused minor pulsing, but this was corrected.

Another upgrade to the test bed could include more use of translation stages. Due to the cost of these components and the time it takes to purchase them, it was difficult to

procure them for the experiment. Additional translation stages will give components such as the mirror and the wavefront sensor a greater degree of freedom when aligning the system. All of theses changes are planned to be compensated for in the next phase of testing. This will include adding several more wavefront sensors, a tip/tilt mirror, and another deformable mirror (see Chapter XI).

X. FUTURE WORK

Adaptive Optics is a new and important area of study. The ability to detect and remove deformations in a laser beam opens the door for all kinds of space applications. That was the idea behind the concept of test bed dedicated to optical refinement. There are many different aspects to satellite communications, however, and adaptive optics alone is not enough to correct for aberrations in the incoming laser source. Jitter plays a large role in the on-board problems experienced when running dedicated optical systems. For this reason, future work will focus on the combination of adaptive optics and adaptive controls.

The optical relay laboratory has developed a unique test bed aimed at correcting disturbances in laser systems. Using an Adaptive Bias Filter, a compensating bias is applied to an adaptive filter allowing rapid convergence in correcting narrow band disturbances[23]. This experimental system uses an Adaptive Delay Filter to the control system to help correlate the error signal with the reference signal. These new control methods, combined with the Linear Quadratic Regulator, help to better reduce disturbances caused by noise injected into an optical beam. The test bed has demonstrated up to a 75% improvement in broadband jitter experienced by an optical beam.

By combining the improvements made in adaptive controls and adaptive optics, the quality of the laser signal could be significantly improved as it travels through both the optical system and the earth's atmosphere. The system designed in this paper is shown below.

[23] Watkins, Joseph. Abstract to doctoral thesis.

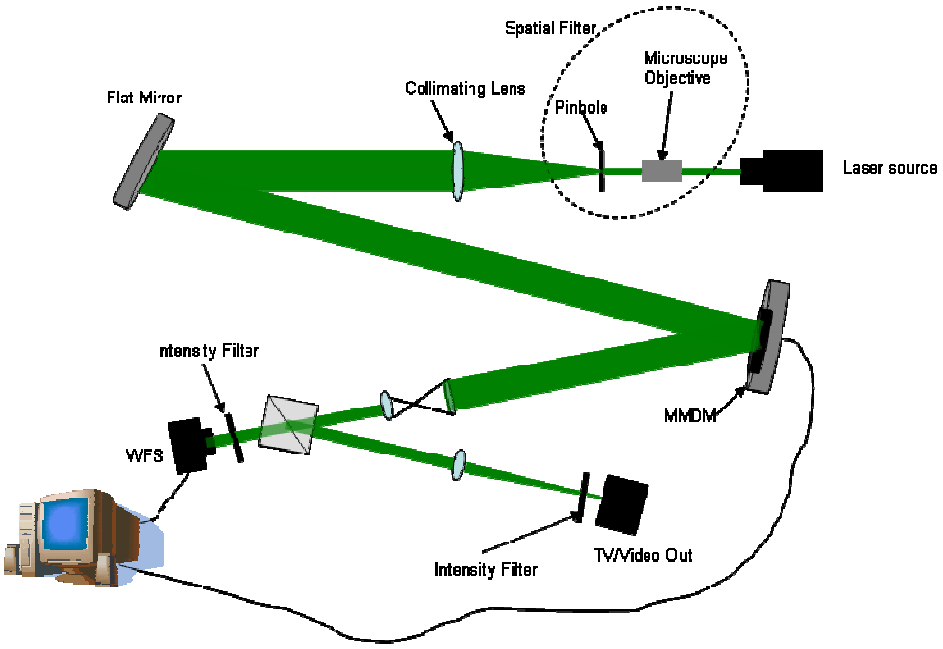

Figure 39. Current AO System

The test bed built in this thesis is as basic as an Adaptive Optics table can get and still function. The wavefront sensor and mirror combined with the software are not accurate above the fourth order level of aberration. This test bed by itself is to be used mainly to test the deformable mirror and verify operation of the wavefront sensor and software. In order to correct for more complies systems, a more robust test bed must be assembled.

The next step to the adaptive optics experiment is to move it to a larger table and infuse it with the adaptive controls test bed. This will require more wavefront sensors and mirrors as shown below.

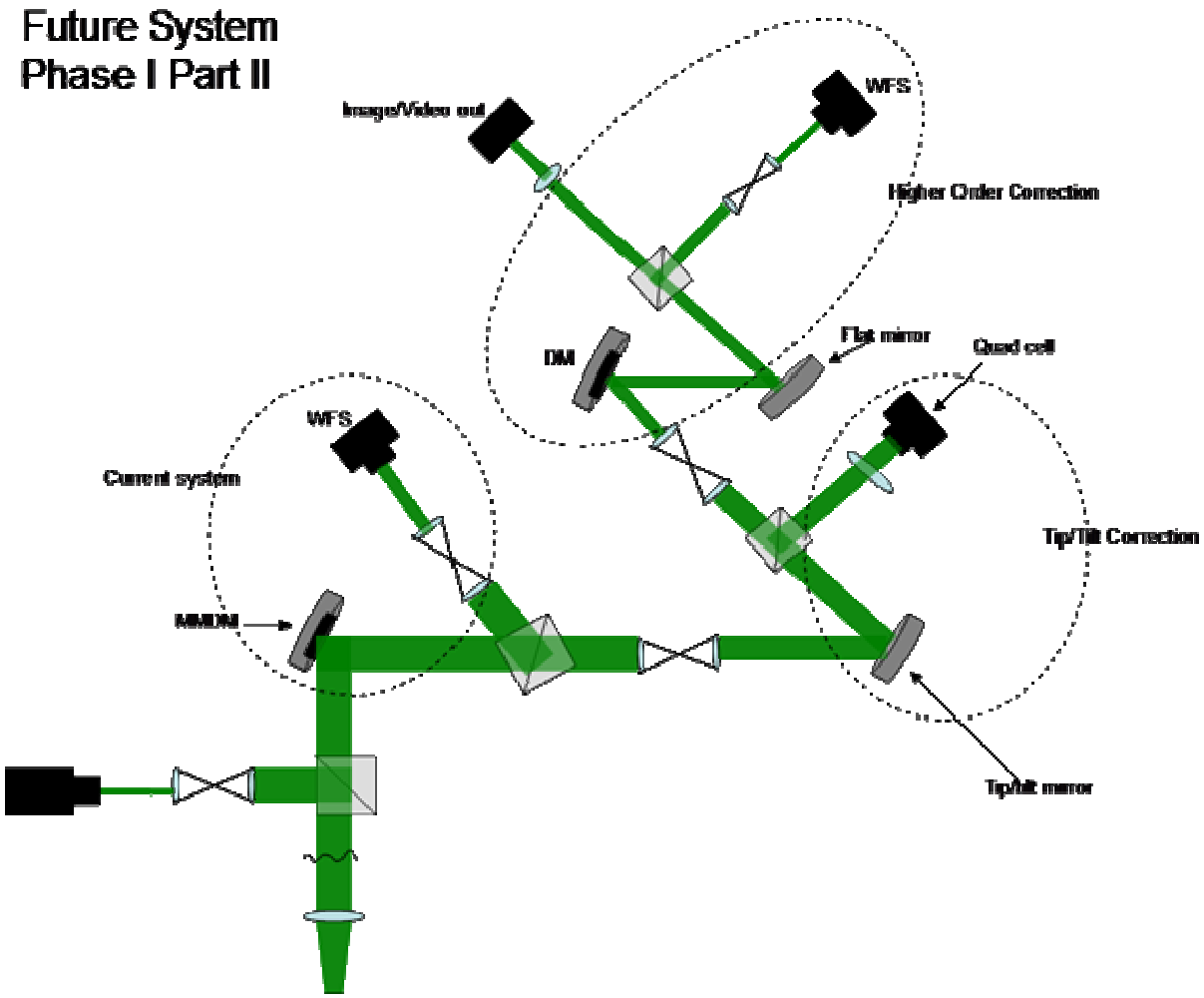

Figure 40. Next Phase of AO System Development

This system requires three different control loops, one to correct the aberrations on the primary mirror (first deformable mirror), one to correct tip/tilt, and one to correct any aberrations that are left over in the system. The video out provides visual monitoring of the corrections as they are being performed. Re-imaging optics are used to relay the pupil to the fast steering mirror and to relay the pupil from the primary mirror to the wavefront sensor to optimize measurements. Several different types of wavefront sensors will be used in order to compare reliability and effectiveness of the sensors and compare data.

The ultimate goal is to model as best as possible the actual telescope system as shown below with an AO system for correction.

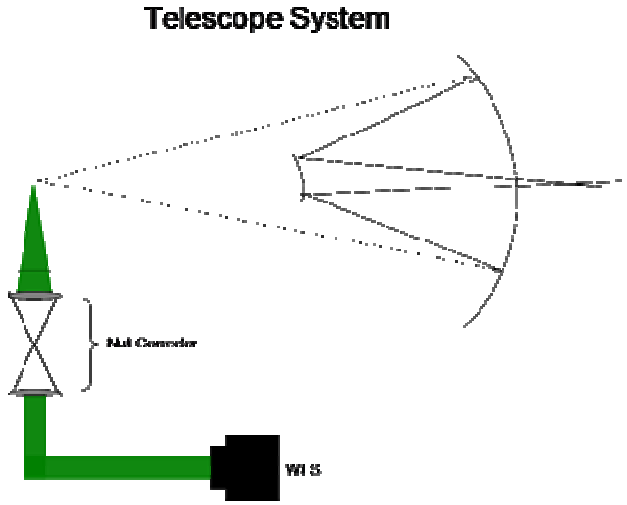

Figure 41. Actual system being modeled

By combining these studies it is hoped to be able to correct for multiple disturbances in a laser beam source. This new study in adaptive optics and adaptive controls will hopefully demonstrate a more accurate correction of laser beam disturbances.

LIST OF REFERENCES

Babcock, Horace. "The Possibility of Compensating Astronomical Seeing". Publications of the Astronomical Society of the Pacific. 65 (October 1953) : 229-236.

Beam Expansion. Department of Physics and Astronomy, The University of Edinburgh, Scotland. 13 August 2005.

Born, Max, and Emil Wolf. Principles of Optics. Cambridge, UK: University Press, 1983.

"First Light for Keck Laser Guide Star." CFAO Newsletters. 2002. Center for Adaptive Optics. 02 October 2005. <http://cfao.ucolick.org/pubs/newsletters/02/firstlight.shtml>

Frazier, Benjamin, and Robert K. Tyson. Field Guide to Adaptive Optics. Washington DC: SPIE Press, 2004.

"High Speed Adaptive Optics System for Use in Free Space Otical Communications." Commerce Business Daily. June 2005. National Electronic Procurement Assistance Center. 30 October 2005. <http://www.cbd-net.com/index.php/search/show/851490>

Johnson, B.K. Optics and Optical Intstruments. New York: Dover Publications, 1960.

"Keck Observatory Laser Guide Star Adaptive Optics System Development." Laser Guide Star Adaptive Optics Program. No Date. Lawrence Livermore National Laboratory. 20 October 2005 http://www.llnl.gov/urp/science/lgs_www/lgs_keck.html>

Kidger, Michael J. Fundamental Optical Design. Bellingham, Washington: SPIE Press, 2002.

Kuhn, Kelin J. Laser Engineering. New Jersey: Prentice Hall Inc., 1998.

Lamberson, Donald L., Edward Duff, Don Washburn, and Courtney Holmberg. Whither High-Energy Lasers? March 2004. Air and Space Power Journal. 15 October 2005. <http://www.airpower.maxwell.af.mil/airchronicles/apj/apj04/spr04/lamberson.html>

Landis, Geoffrey A., and Larry H. Westerlund. Laser Beamed Power: Satellite Demonstration Applications. 1992. NASA Glenn Research Center. 30 September 2005. <http://powerweb.grc.nasa.gov/pvsee/publications/lasers/IAF92_0600.html>

Max, Claire. Laser Guide Star Adaptive Optics Program. January 1997. Lawrence Livermore National Laboratory. 20 October 2005. <http://www.llnl.gov/urp/science/lgs_www/lgs.html>

McCartney, Earl J. Optics of the Atmosphere. New York: John Wiley & Sons, Inc., 1976.

McMahon, Matt. Adaptive Optics for Retinal Imaging. 2003. 13 September 2005. < http://www.mattmcmahon.com/ao.html>

Midwinter, John E. and Frits Zernike. Applied Nonlinear Optics. New York: John Wiley & Sons, Inc., 1973.

Newton, Sir Isaac. Optiks. New York: Dover Publications, 1952.

Newton, Sir Isaac. The Principia: Mathematical Principles of National Philosophy. Los Angeles, CA: University of California Press, 1999.

"NRL Collaborates with Magdalena Ridge Observatory Consortium to Build New Observatory". NRL Press Release. 2001. Naval Research Laboratory. 17 September 2005. <http://www.nrl.navy.mil/pao/pressRelease.php?Y=2001&R=37-01r>

OKO Technologies. 37(19) Channel Micromachined Deformable Mirror System: Technical Passport. Delft, The Netherlands: OKO Technologies, 2003.

O'Shea, Donald C., W. Russell Callen, and William T. Rhodes. Introduction to Lasers and Their Applications. Philippines: Addison-Wesley Publishing Company, Inc., 1977.

Pedrotti, Frank L., S. J. and Leno S. Pedrotti. Introduction to Optics. New Jersey: Prentice Hall Inc., 1993.

Shen, Y. R. The Principles of Non-Linear Optics. New York: John Wiley & Sons, Inc., 1984.

Silfvast, William T. Laser Fundamentals. Cambridge, UK: University Press, 2003.

Skilling, Hugh Hildreth. Fundamentals of Electric Waves. Malabar, FL: Robert E. Krieger Publishing Company, 1974.

Schwiegerling, J. Adaptive Optics, LASIK and Wavefront Sensing. September 2001. OpticsReport. 27 September 2005. <http://www.opticsreport.com/content/article.php?article_id=1005>

Tyson, Robert K. Principles of Adaptive Optics. San Diego, CA: Academic Press, 1998.

Vdovin, Gleb and Mikhail Loktev. FrontSurfer Wavefront Analysis and Control System, version 1.3. Delft, The Netherlands: OKO Technologies, 2003.

INITIAL DISTRIBUTION LIST

1. Defense Technical Information Center
   Ft. Belvoir, VA

2. Dudley Knox Library
   Naval Postgraduate School
   Monterey, CA

3. Dr. Brij Agrawal
   Naval Postgraduate School
   Monterey, CA

4. Dr. Don Walters
   Naval Postgraduate School
   Monterey, CA

5. Sergio Restaino
   Naval Research Laboratory
   Kirtland AFB
   Albuquerque, NM

6. Ty Martinez
   Naval Research Laboratory
   Kirtland AFB
   Albuquerque, NM